Michigan State University

National Superconducting Cyclotron Laboratory

SHELL MODEL STRUCTURES OF LOW-LYING EXCITED STATES IN ^{6,7}Li

S. KARATAGLIDIS, B. A. BROWN, K. AMOS,
and P. J. DORTMANS

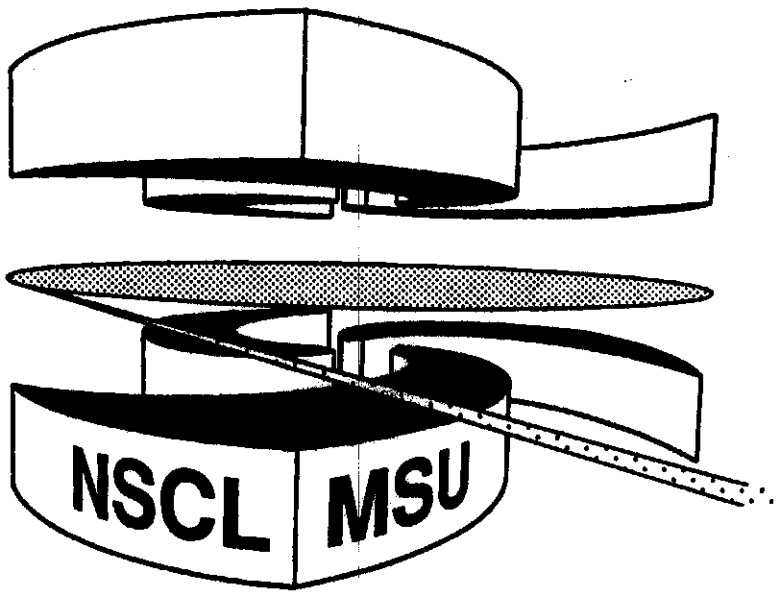

MSUCL-1053

DECEMBER 1996

Shell model structures of low-lying excited states in ^{6,7}Li

S. Karataglidis, B. A. Brown,

National Superconducting Cyclotron Laboratory, Michigan State University, East Lansing, Michigan, 48824-1321

K. Amos, and P. J. Dortmans,

School of Physics, University of Melbourne, Parkville 3052, Victoria, Australia.

Abstract

Electron and intermediate energy proton scattering data from ^{6}Li and ^{7}Li, both elastic and inelastic, have been analyzed using wave functions obtained from shell model calculations involving spaces ranging from the conventional $0\hbar\omega$ space to the $(0 + 2 + 4)\hbar\omega$ one. The results, along with those of the static and dynamic properties of the low lying spectra of the nuclei, allow for a strict assessment of the wave functions, as well as giving an indication of possible cluster-like behavior in those systems.

I. INTRODUCTION

While the shell model is the most fundamental of nuclear structure models, states in light nuclei also have been described successfully in terms of clusters. Indeed, Wildemuth and Tang [1] have shown a correspondence between the cluster and shell models, the clusters arising naturally as correlations out of the shell model Hamiltonian. For light nuclei, the cluster model reduces the many-body problem to a few-body one, with interactions occurring between the clusters. These interactions involve particle exchanges, since the nucleons may still be considered somewhat freely moving, with their motion not strictly confined to the clusters themselves. Such is the relation of the cluster model to the shell model. For a realistic shell model then, one may expect some evidence of clustering in the wave functions for those systems in which the cluster model is valid.

A good place to look for this behavior is in the ^{6}Li and ^{7}Li nuclei. Both of these have been described successfully in terms of clusters [2], as $\alpha+d$ in the case of ^{6}Li (or as $\alpha+p+n$ in a three-body description [3]), and $\alpha+t$ for ^{7}Li, although other two-cluster configurations are possible [2]. The simple $0\hbar\omega$ shell model descriptions of these nuclei automatically contain such clustering: the $0s$-shell inert core is the α particle, while the valence nucleons in the $0p$-shell naturally form the other cluster. More recently, large space multi-$\hbar\omega$ shell models have been constructed for these nuclei [4]. Such are required if a shell model approach is to model cluster effects realistically [5].

The purpose of the present work is to investigate to what extent current shell model wave functions for ^{6}Li and ^{7}Li exhibit "clustering" behavior, i.e. the extent of correlations which arise from the multi-$\hbar\omega$ configurations, and as may be evident in electromagnetic and scattering properties. The wave functions are obtained in all the available model spaces; from the $0\hbar\omega$ through to the $(0+2+4)\hbar\omega$ space. Those wave functions then are used in calculations of the ground state properties and in analyses of complementary elastic and inelastic electron and proton scattering data. These provide a stringent test of the nuclear wave functions, and, as higher $\hbar\omega$-excitations are added to the model space, allows for the

investigation of clustering behavior. Such additions provide the renormalization to the $0\hbar\omega$ model space one associates normally with core polarization corrections. In the case of ^{12}C [6], analyses of such complementary scattering data using realistic wave functions gave very good agreement with experiment, without the need for any corrections to the wave functions obtained.

A related question to the analyses of the scattering data is whether a distorted wave approximation (DWA) approach to the analysis of proton scattering data is sufficient to determine the scattering properties independently of the use of any data from electron scattering. This is important for an understanding of the experimental results now available for the scattering of ^{11}Li from hydrogen [7], and which, in the inverse kinematics, provides proton scattering data from that halo nucleus. Similar experiments also are being planned for proton scattering from other exotic nuclei, for which electron scattering form factors are not attainable at present (although such experiments are being planned for RIKEN [8]).

The paper is organized as follows. The nuclear structure and the nuclear wave functions are described in detail in Sect. II. The formalism for obtaining the electron and proton scattering observables is described in Sect. III. Results are presented in Sect. IV, while the conclusions are contained in Sect. V.

II. MODELS OF STRUCTURE

We consider shell model wave functions within the $0\hbar\omega$, $(0+2)\hbar\omega$, $(0+2+4)\hbar\omega$, and $(0+2+4+6)\hbar\omega$ model spaces. However, within the largest of these, because of the dimension of the space, only a calculation of the ground state properties has been made. The choice of model space dictates the choice of interaction and, specifically, the ones used were

- the Cohen and Kurath $(6-16)$2BME interaction (CK) [9] for the complete $0\hbar\omega$ model space,
- the MK3W interaction [10] for the complete $(0+2)\hbar\omega$ shell model space, and

- (c) the G-matrix interaction of Zheng *et al.* [4] for the complete $(0+2+4)\hbar\omega$ (hereafter known as Z4) model space.

For the calculations of the ground state properties only, wave functions were obtained using the interaction of Zheng in a $(0+2+4+6)\hbar\omega$ model space.

The removal of center-of-mass spuriosity is straightforward for calculations performed in complete shell model spaces. In all calculations presented herein, the removal of such spuriosity has been done by adding the appropriate center-of-mass Hamiltonian from the shell model Hamiltonian before diagonalization and projecting the center-of-mass eigenstates upwards in the energy spectrum (see, for example, [11]).

It should be noted that the MK3W interaction was designed only to treat the complete $0\hbar\omega$ and $1\hbar\omega$ spaces within the same basis. However, that interaction has been used with some success in calculations of the states of ^{12}C within the complete $(0+2)\hbar\omega$ space [6]. We have made calculations also within the complete $0\hbar\omega$ and $(0+2)\hbar\omega$ spaces using the G-matrix interactions of Zheng [12] as well to compare with the results found using the fitted (phenomenological) interactions. All calculations of the wave functions and of the one body density matrix elements (OBDME), which specify the structure changes in inelastic scattering events, were carried out using the code OXBASH [13].

The $J^\pi;T$ states considered in this study are the ground, $3^+;0$ (2.186 MeV), and $0^+;1$ (3.563 MeV) in ^{6}Li, and the ground, $\frac{1}{2}^-;\frac{1}{2}$ (0.478 MeV) and $\frac{7}{2}^-;\frac{1}{2}$ (4.630 MeV) states in ^{7}Li. The ground state binding energies obtained from the $(0+2+4)\hbar\omega$ calculation are -27.237 MeV and -34.127 MeV for ^{6}Li and ^{7}Li respectively, as compared to the measured values [14] of -31.966 MeV and -39.244 MeV respectively. Both nuclei are less bound by about 7 MeV in the model as compared to experiment. The results obtained using the full G matrix [4] are -30.525 MeV for ^{6}Li in the full $(0+2+4+6)\hbar\omega$ model space, and -37.533 MeV for ^{7}Li in the full $(0+2+4)\hbar\omega$ space. The relative binding energy predicted in our $(0+2+4)\hbar\omega$ model is 6.890 MeV and is quite close to the measured value of 7.278 MeV. The ground state wave functions in the $(0+2+4)\hbar\omega$ model space are

$$|^6\mathrm{Li}\rangle = 76.62\%\,|0\hbar\omega\rangle + 11.93\%\,|2\hbar\omega\rangle + 11.45\%\,|4\hbar\omega\rangle \tag{1}$$

and

$$|^7\mathrm{Li}\rangle = 74.01\%\,|0\hbar\omega\rangle + 14.16\%\,|2\hbar\omega\rangle + 11.83\%\,|4\hbar\omega\rangle\,, \tag{2}$$

indicating for both nuclei that the ground state is roughly 75% $0\hbar\omega$ in character.

The excited states are listed in Table I, together with the excitation energies obtained from the various shell model calculations. From those results, the importance of increasing the size of the model space is evident. For example, the energy of the $\frac{1}{2}^-$ (0.478 MeV) state in ^{7}Li in the $0\hbar\omega$ model space is 0.115 MeV, obtained using the Zheng interaction. Inclusion of $2\hbar\omega$ excitations in the model space gives 0.472 MeV for that same interaction, suggesting a convergence in the eigenvalue to the observed value. The inclusion of the $4\hbar\omega$ excitations provides still better agreement, with the result found using the Zheng interaction being in excellent agreement with the measured spectrum, and our results obtained with the Zheng interaction agree well with those quoted by Zheng *et al.* [4]. Such is also the case with the other states, although it is true that the use of the MK3W interaction in the $(0+2)\hbar\omega$ space for the ^{6}Li spectrum actually worsens the agreement with the experiment. In that case the $0^+;1$ state is lower in excitation energy than the $3^+;0$ state, due in part to the use of the Cohen and Kurath $(8-16)$2BME interaction [9] for the $0p$-shell part of the MK3W interaction.

There are other questions in regard to our calculations made using the Zheng interactions. For example, the multi-valued nature of the G matrix interaction [4] has not been implemented as yet in OXBASH. The excellent agreement with experiment, and with the values obtained using the full G matrix [4], suggests that such is not a significant problem. Also, OXBASH is designed to work in bases encompassing the complete $(0+2+4)\hbar\omega$ space, from the $0s$ up to, and including, the $0h1f2p$ shells (21 orbitals). The higher shells required for a complete $(0+2+4+6)\hbar\omega$ space are not included. This may affect the results we obtain for the ground state properties.

In the predictions of the ground state properties and of scattering, as in the nuclear structure information, one also requires the specification of the single particle (SP) wave functions. We have used SP functions of harmonic oscillator (HO) and Woods-Saxon (WS) form. The latter, which may be most appropriate when analyses are made of scattering properties, were obtained as solutions to the Schrödinger equation with the potential

$$V = V_0 \left(1 + 2\lambda [\mathbf{l} \cdot \mathbf{s}] \left(\frac{\hbar}{m_\pi c} \right)^2 \frac{1}{r} \frac{d}{dr} \right) f(r, R, a) \ , \tag{3}$$

where, with $R = r_0 A^{1/3}$,

$$f(r, R, a) = \frac{1}{1 + \exp\left(\frac{r-R}{a}\right)}. \tag{4}$$

Both the oscillator energies and WS parameters were determined from fitting longitudinal elastic electron scattering form factors. For the unbound states (those above the $0p$ shell), wave functions of HO form were used. In the case of the calculations of the ground state properties using the Zheng wave functions [4], however, we have chosen to use HO functions using the oscillator energy specified by the G-matrix interaction ($\hbar\omega = 14$ MeV).

III. ELECTRON AND PROTON SCATTERING

The propriety of the various models considered herein are tested by their use in analyses of electron scattering form factors and of proton scattering data. The use of the OBDME in analyses of the electron scattering form factors to each of the states in ^{6,7}Li complements those of the proton scattering observables thus providing a stringent test of the wave functions from which the OBDME are determined.

The calculations of the form factors for electron scattering are based upon the formalism of deForest and Walecka [15], but we have modified their specification of the transverse electric operator by using Siegert's theorem in the way indicated by Friar and Haxton [16] so that the effects of meson exchange currents (MEC) are incorporated implicitly. We use the $T^{el'}$ form for the operator effecting the transverse electric transition [16,17]. That form,

incorporating MEC in the long wavelength limit, has been found to be the most appropriate for use with $0\hbar\omega$ structure wave functions [17]. Also, where appropriate, bare charges and the one-body current densities have been used to specify the one-body operators required in the calculations of the longitudinal and transverse form factors. We have neglected explicit MEC corrections to the transverse magnetic form factors, as those corrections are expected to have an appreciable effect only for momentum transfers above 3 fm^{-1} [18]. Thus the electromagnetic operators are all one-body in character.

To calculate the many-body matrix elements of one-body operators, a cofactor expansion of the nuclear wave function is used, viz.

$$|\Psi\rangle = \frac{1}{\sqrt{A}} \sum_{\alpha_1, m_1} |\varphi_{\alpha_1, m_1}\rangle \, a_{\alpha_1, m_1} \, |\Psi\rangle \,, \tag{5}$$

where $\alpha_i = \{n_i, l_i, j_i, \rho_i\}$, with ρ specifying either a proton or a neutron. By summing the one-body operator over the individual nucleons and using the Wigner-Eckart theorem, the (reduced) many-body matrix element of the one-body operator becomes

$$\left\langle J_f \left\| \hat{O}_I \right\| J_i \right\rangle = \frac{1}{\sqrt{2I+1}} \sum_{\alpha_1 \alpha_2} \left\langle \varphi_{\alpha_2} \left\| \hat{O}_I \right\| \varphi_{\alpha_1} \right\rangle S_{\alpha_1 \alpha_2 I}, \tag{6}$$

where $S_{\alpha_1 \alpha_2 I}$ are the (singly) reduced OBDME, viz.

$$S_{\alpha_1 \alpha_2 I} = \left\langle J_f \left\| \left[a^{\dagger}_{\alpha_2} \times \tilde{a}_{\alpha_1} \right]^I \right\| J_i \right\rangle . \tag{7}$$

For the cases of interest the OBDME have been tabulated [19].

The calculations of the intermediate energy proton scattering observables follow the fully microscopic ones done in the case of ^{12}C [6]. There are three essential ingredients one must specify to make such a calculation of the elastic and inelastic proton scattering. First the OBDME, as used in both the the inelastic electron scattering calculations, are obtained from the selected nuclear structure. Second, the single particle wave functions describing the nucleon bound states must be chosen, and for our calculations these were the same as those used in the analyses of the electron scattering form factors. Finally, an effective interaction between the projectile nucleon and each and every nucleon in the target must be chosen.

That effective interaction [6] is one whose double Bessel transform accurately maps a set of nucleon–nucleon (NN) g matrices [20]. These density dependent g–matrices are solutions of the Brueckner-Bethe-Goldstone equations in which a realistic NN potential defines the basic pairwise two nucleon interaction. For these we have used the Paris NN interaction [21]. Those g matrices, for a range of incident proton energies, are available elsewhere [22]. The complex, fully nonlocal optical potentials used in the nonlocal Schrödinger equation code DWBA91 [23], to obtain the differential cross sections and analyzing powers, were obtained by folding the ground state OBDME with those same g matrices. Recoil of the target nucleus is an important feature of these optical model calculations, as are the non–zero multipoles in the elastic scattering as the target are not spin zero nuclei. Both effects have been included in all calculations.

As the optical potential is dependent on the OBDME found using the ground state as both the initial and final multiparticle states of Eq. (7), the quality of the results of the proton scattering calculations will be determined by the quality of the wave functions. Note that while most of such OBDME effectively are nucleon shell occupancy values, off–diagonal elements (when the principal quantum number changes) must be taken into account. That there is excellent agreement with both electron and proton scattering data when reasonable wave functions are used has been illustrated in the case of ^{12}C [6], for both elastic and inelastic scattering.

IV. RESULTS

A. Ground state properties of ^{6,7}Li

One can assess the cluster-like behavior of the shell model wave functions by examining the ground state properties predicted by each model. Such are shown in Tables II and III wherein the root–mean–square (r.m.s.) charge radii, magnetic moments, and quadrupole moments of the ground states of ^{6}Li and ^{7}Li are compared with values predicted using

the wave functions obtained from the complete $0\hbar\omega$, $(0+2)\hbar\omega$, $(0+2+4)\hbar\omega$, and the incomplete $(0+2+4+6)\hbar\omega$ model spaces. The Zheng interaction [4,12] was used in all cases in Table II, with SP wave functions of HO form ($\hbar\omega = 14$ MeV), to investigate the change in those observables with increasing the size of the model space only. The results obtained from the CK, MK3W, Zheng interactions in the complete $0\hbar\omega$, $(0+2)\hbar\omega$, and $(0+2+4)\hbar\omega$ model spaces are shown in Table III for comparison. The data for the r.m.s. radii were taken from Ref. [24], while those for the magnetic and quadrupole moments were taken from Ref. [14].

For ^{6}Li, and for ^{7}Li, the r.m.s. radius is predicted adequately by all model calculations and generally is insensitive to the addition of higher-$\hbar\omega$ excitations to the $0\hbar\omega$ model space. The effect of increasing the size of the model space is more noticeable in the magnetic and quadrupole moments. There is a dramatic decrease in the calculated value of the magnetic moment in adding $2\hbar\omega$ excitations to the model space, from 0.869 n.m. to 0.848 n.m., compared with the experimental value of 0.822 n.m. Proceeding from the $(0+2)\hbar\omega$ space to the $(0+2+4+6)\hbar\omega$ there is a steady decrease in the value of the magnetic moment, but that change is more gradual. There is an additional correction to the $(0+2+4+6)\hbar\omega$ value of 0.840 n.m. of -0.007 n.m. [25] due to higher-$\hbar\omega$ core polarization effects (-0.009 n.m.), meson-exchange currents (0.033 n.m.) and relativistic effects (-0.031 n.m.), giving a final value of 0.833 n.m., which is comparable to the experimental one. In the case of the quadrupole moment, the effect of increasing the model space is most dramatic. There is little change to the result of -0.264 e fm^2, obtained using the $0\hbar\omega$ space wave function, when $2\hbar\omega$ excitations are allowed. However, adding $4\hbar\omega$ excitations gives a value of -0.012 e fm^2, a correction of more than an order of magnitude, which, in comparison to the experimental value of -0.083 e fm^2, actually overcompensates. This is exacerbated in the result obtained using the $(0+2+4+6)\hbar\omega$ space ground state wave functions with which the calculated moment is positive. This is due in part to the use of the incomplete space, which encompasses only 6 major shells. The results obtained in the complete space is -0.067 e fm^2 [4]. While our result is not calculated in the complete space, this illustrates that large variations in the prediction

of the (small) quadrupole moment may be produced with small perturbations added to the shell model wave functions.

In comparison, the result of the r.m.s. radius for ^{6}Li obtained using the CK interaction, as shown in Table III is comparable to that obtained using the Zheng interaction in the $0\hbar\omega$ model space. However, the results for the magnetic and quadrupole moments differ significantly. The magnetic moment predicted using the CK wave functions is closer in agreement to the measured value than that obtained using those from the Zheng interaction, while the quadrupole moment is much worse. The results for all three quantities predicted using the wave functions obtained from the MK3W interaction all differ markedly from the corresponding values obtained using the Zheng interaction. The r.m.s. radius is much closer to the measured value, although the agreement between the predicted and measured magnetic and quadrupole moments is much worse.

In the ground state of ^{7}Li, as for ^{6}Li, the effect of changing the size of the model space is most apparent in the calculation of the quadrupole moments. For the magnetic moment, there is little change in the predicted value when the size of the space is increased. Indeed, above the $(0+2)\hbar\omega$ space, the additional core polarization corrections actually give results which diverge away from the measured value of 3.256 n.m. For the result obtained in the $(0+2+4+6)\hbar\omega$ space, the additional corrections [25] coming from higher $\hbar\omega$ excitations (-0.025 n.m.), contributions from the Δ (0.014 n.m.), meson exchange currents (0.095 n.m.), and relativistic effects (-0.091 n.m.), gives a total value of 2.999 n.m. But it is in the calculation of the quadrupole moment that we notice the most dramatic changes. None of the results from using the differing model spaces reproduce the measured value of -4.06 e fm^2, with the $0\hbar\omega$ result giving the worst value of -1.68 e fm^2. Adding $2\hbar\omega$ excitations gives a value of -2.43 e fm^2 which represents the largest correction to the $0\hbar\omega$ result. The result obtained in the $(0+2+4)\hbar\omega$ space is -2.63 e fm^2, as compared to -2.372 e fm^2 obtained using the complete multi-valued G-matrix [4]. Increasing the size of the model space gives further corrections, with a value of -2.85 e fm^2 being obtained in the (incomplete) $(0+2+4+6)\hbar\omega$ space.

As for ^{6}Li, the comparison between the results obtained using the fitted interactions and those obtained using the G matrix are interesting. In the case of the r.m.s. radius, the value obtained using the CK interaction is the same as that obtained using the Zheng interaction. However, that is not the case when comparing the results obtained in the $(0+2)\hbar\omega$ space. The r.m.s. radius obtained using the MK3W wave functions is significantly larger than that obtained using the Zheng wave functions, and is much closer to the measured value. Both the magnetic moments obtained using the CK and MK3W wave functions are larger than those obtained using the Zheng interaction, including that result obtained in the $(0+2+4)\hbar\omega$ model space, and are much closer to the measured value. In the case of the quadrupole moment, the value obtained using the CK interaction is comparable to that obtained using the Zheng interaction, while the value obtained from the MK3W interaction is worse in comparison to the measured value.

Note that the single particle wave functions used in the calculations of the ground state properties are not the same as from those used in the scattering calculations to be discussed later. However using those alternate wave functions (Table IV) in the calculations of the ground state observables does not significantly change our results.

B. Scattering: ^{6}Li

In all of the following diagrams, unless otherwise stated, the results obtained using the wave functions of the $(0+2+4)\hbar\omega$, $(0+2)\hbar\omega$, and $0\hbar\omega$ model spaces are given by the solid, dashed, and dot-dashed lines, respectively.

The elastic electron scattering form factors for ^{6}Li are displayed in Fig. 1. In Fig. 1(a), the longitudinal elastic form factor data of Suelzle *et al.* [26] (circles) and of Li *et al.* [27] (squares) are compared to the results we have obtained using the Z4, MK3W, and CK shell models, and with WS bound state wave functions. The parameter values of the WS potential used to obtain those single particle wave functions for ^{6}Li (and for ^{7}Li) are given in Table IV, along with the oscillator energies defining those of harmonic oscillator form.

Concomitant with the quadrupole moment of ^{6}Li being small (see the discussion above), the $C2$ contribution to the form factor is orders of magnitude smaller than that of $C0$. That is displayed in Fig. 1(b). Therein, the data are compared to the total form factor obtained using the Z4 shell model (solid line), and its $C0$ (dashed line) and $C2$ (dot-dashed line) components. Hence, the results presented in Fig. 1(a) are just the $C0$ contributions to the form factor. The dramatic difference between the results found using the structure of the fitted models and using the structure based on the G matrix, illustrated by the different single particle wave function parameter sets, may be due to the differences in the nuclear wave function influencing the choice of those single particle wave functions to reproduce the longitudinal elastic scattering form factor.

The transverse $M1$ elastic electron scattering form factor for ^{6}Li is presented in Fig. 1(c) wherein the data of Bergstrom *et al.* [28] (circles) and of Lapikás [29] (squares) are compared to the results of our calculations made using the wave functions from the Z4, MK3W, and CK shell models. The single particle wave functions used were those determined from the analysis of the longitudinal form factor, as is the case with the analyses of the inelastic scattering data. With all three models we are able to predict the magnitude of the form factor well, especially below the minimum at 1.3 fm^{-1}, but the result obtained using the CK wave functions fails to reproduce the position of the minimum. Both the MK3W and Z4 models reproduce that minimum well, but only with the Z4 model can we predict the shape of the form factor at higher momentum transfers adequately.

The results of our calculations of the elastic scattering for 200 MeV protons from ^{6}Li are compared with the data of Glover *et al.* [30] in Fig. 2. The cross sections are shown in the top segments while the analyzing powers are given in the bottom ones. The results for the $(0+2)\hbar\omega$ and $(0+2+4)\hbar\omega$ models are given in the left and right hand panels respectively. The single particle bound states were specified either as HO (dashed curves) or WS (solid curves) wave functions, identified by the parameter values given in Table IV. The higher ($I > 0$) multipoles that are possible in this scattering were calculated in the DWA using DWBA91 [23]. This is in accordance with the calculations presented in Ref. [30], and we find

similar contributions to those calculations from the higher multipoles. Recoil corrections to the cross section and analyzing power have also been included and when such is done with both the OBDME from the $(0+2)\hbar\omega$ and $(0+2+4)\hbar\omega$ models, we find very good agreement with the both the cross-section and analyzing power data. Taken together with the very good agreement achieved with the elastic electron scattering data, this suggests that the ground state wave functions obtained in the multi-$\hbar\omega$ spaces have converged.

The longitudinal inelastic electron scattering form factor to the $3^+;0$ (2.185 MeV) state is displayed in Fig. 3(a), wherein the data of Bergstrom *et al.* [31] (circles), Yen *et al.* [32] (squares), Bergstrom and Tomusiak [33] (crosses), and Hutcheon and Caplan [34] (triangles) are compared to the results obtained from our calculations. The form factor, as calculated using all shell models, is dominated by the $C2$ component, while the $C4$ component is found to be negligible. With the MK3W and Z4 models, our calculated results reproduce the magnitude of the measured form factor above 1 fm^{-1}, as both contain strength from transitions outside of the $0p$-shell which enhance the $C2$ strength. Such are missing in the $0\hbar\omega$ model. The $(0+2+4)\hbar\omega$ model structure is most favored as there is almost exact agreement with the data in that region of momentum transfer. However, the B(E2) value for the associated γ–decay of this $3^+;0$ state is 9.3 ± 2.1 e^2 fm^4 [14,32], and the values obtained by calculation using the CK, MK3W, and Z4 models of structure are significantly smaller. Those values are given in the top line of Table V. So far as the γ–decay is concerned all calculations require a substantial renormalization to reproduce the measured value. That is confirmed by our predictions of the electron scattering form factor at low momentum transfer. Below 1 fm^{-1} all of the calculated results are less than observation. Yet that degree of renormalization is not suggested by the results of the calculations of the form factor at higher momentum transfer. While this suggests that the internal (nucleon) dynamics of the nucleus are well described by the inclusion of higher $\hbar\omega$ excitations in the model space, such cannot account for the asymptotics of the structure. At large radii, which most influence scattering at low momentum transfer, the clustering of the wave function is not reproduced by the shell model in which up to $4\hbar\omega$ excitations are included. This deviation of all the

calculated results away from the data is illustrated further in Fig. 3(b) which displays the B(E2↓,q) value as a function of momentum transfer for the $3^+;0$ (2.186 MeV) state in ^{6}Li, as determined from the measured and predicted longitudinal inelastic form factors. This is achieved by removing from the form factor most of the dependence on the momentum transfer, according to the transformation given by Brown, Radhi, and Wildenthal [35]. The B(E2↓) value as related to the associated γ–decay is given by the $q = 0$ intercept.

The cross sections and analyzing powers obtained from the various shell models for the inelastic scattering of 200 MeV protons to the $3^+;0$ (2.186 MeV) state in ^{6}Li are compared to the data of Glover *et al.* [30] in Fig. 4. HO single particle wave functions were used to find the results shown in the left hand panels while those of WS form were used to obtain the results displayed in the right hand ones. The cross sections displayed are the sum of all possible angular momentum transfers which may contribute. Consistent with the analysis of the inelastic electron scattering form factor, the $I = 2$ component is the most dominant. It is evident from Fig. 4 that the result found using the simple $0\hbar\omega$ model is deficient. The larger space structures lead to cross sections almost an order of magnitude greater than that, apart from the region around 20° which is still too weak. This problem at low momentum transfer is consistent with the analyses of the inelastic electron scattering data to this state. Note that even the predicted shape found using the simplest structure changes with increase in the space. The analyzing power varies in a similar way with either large basis model calculations well reproducing the data. We note that with the increases to the model space, the $I = 2$ scattering amplitudes are most enhanced to give improved fits to the data.

The transverse $M1$ inelastic electron scattering form factor to the $0^+;1$ state in ^{6}Li is displayed in Fig. 5. Therein, the data of Bergstrom *et al.* (circles [31] and squares [36]) are compared to the results of our calculations made using all three shell model interactions. Both the MK3W and Z4 calculations are able to reproduce the form factor at low momentum transfer, and also the position of the minimum at 1.4 fm^{-1}. The CK model calculation, on the other hand, overpredicts the low–q data and places the minimum at too large a value of momentum transfer.

In Fig. 6, the cross sections and analyzing powers obtained for the excitation of the $0^+;1$ (3.563 MeV) state in ^{6}Li from the inelastic scattering of 200 MeV protons are compared with the data of Glover *et al.* [30]. Single particle wave functions of HO form (left-hand panels) and WS form (right-hand panels) were used as before. In this case, each result is observably different and clearly the largest space calculations best reproduce the data.

C. Scattering: ^{7}Li

As for the diagrams for ^{6}Li, unless otherwise stated, the results obtained using the $(0+2+4)\hbar\omega$, $(0+2)\hbar\omega$, and $0\hbar\omega$ model spaces are given by the solid, dashed, and dot-dashed lines respectively.

The elastic electron scattering form factors for ^{7}Li are displayed in Fig. 7. The longitudinal elastic scattering form factor data of Suelzle *et al.* [26] (circles) and of Lichtenstadt *et al.* [37] (squares) are compared in Fig. 7(a) to the results of the calculations made using the WS single particle wave functions (Table IV). All the calculations reproduce the form factor well, although the data above 3 fm^{-1} allow for some variation between the results which is appreciable. For this reason we restrict our assessment of the models to be based upon the data at momentum transfers below 3 fm^{-1}. Unlike ^{6}Li, there is a substantial contribution from the $C2$ component of the form factor, as displayed in Fig. 7(b). This is due to the much larger quadrupole moment for the ground state of ^{7}Li (see the discussion above). Note that this component is necessary to achieve the fit to the form factor in the region between 2 and 3 fm^{-1}. Calculations of the form factors using HO wave functions, as defined in Table IV, also reproduce the form factor up to 3 fm^{-1}. At large momentum transfers, the form factor is always underpredicted since the HO wave functions do not contain realistic high momentum components. The WS forms are better in that regard.

The transverse elastic electron scattering form factor for ^{7}Li is displayed in Fig. 7(c). Therein the data of Lichtenstadt *et al.* [37] (circles) and van Niftrik *et al.* [38] (squares) are compared to the results of the calculations made using the three models of structure. All

model calculations predict the form factor up to 2.5 fm^{-1}. At higher momentum transfers the $(0+2)\hbar\omega$ model underpredicts the data. The $0\hbar\omega$ and $(0+2+4)\hbar\omega$ model results, however, are more consistent with the data. It should be noted that the results obtained using the Zheng interaction in the $0\hbar\omega$ and $(0+2)\hbar\omega$ model spaces agree with those results based on the fitted interactions, and so are not displayed. Such calculations were also made for the inelastic scattering form factors with very similar results obtained in each model space using the disparate interactions. The components contributing to the transverse form factor, as calculated in the $(0+2+4)\hbar\omega$ model space, are shown in Fig. 7(d), wherein the total, $M1$ and $E2$ components are displayed by the solid, dashed and dot-dashed lines respectively. The low momentum transfer part of the form factor is dominated by the $M1$ component, while the $E2$ component dominates between 1 and 3 fm^{-1}. Above that momentum transfer both components are comparable in strength.

The results for the elastic scattering of 200 MeV protons from ^{7}Li are compared with the data of Glover *et al.* [39] in Fig. 8 for which the specifications follow those set out in the discussion of Fig. 2. As with the results for the elastic scattering from ^{6}Li, the contributions from the higher multipoles, calculated in the DWA, and recoil corrections have been included. This has resulted in the very good agreement observed with the data suggesting, as with ^{6}Li, that the multi-$\hbar\omega$ wave functions for the ground state are appropriate.

The inelastic electron scattering form factors to the $\frac{1}{2}^-$ (0.478 MeV) state in ^{7}Li are displayed in Fig. 9. The longitudinal form factor data of Lichtenstadt *et al.* [37] (circles) and of van Niftrik *et al.* [38] (squares) are compared to the results of the calculations made using the various shell models in Fig. 9(a). The result obtained in the $0\hbar\omega$ space using the CK wave functions fails to reproduce the magnitude of the data. The result obtained using the Zheng interaction in the $0\hbar\omega$ space is similar to that obtained using the CK one indicating inadequacy with a $0\hbar\omega$ shell model description of the state. Inclusion of higher $\hbar\omega$-components in each case supplies the necessary strength to reproduce th data. For $q > 3$ fm^{-1}, MEC corrections to the charge density operator may be required to reproduce those data (see, e.g. Ref. [40]).

The B(E2) value for this transition is 16.4 e^2 fm^4 [14], and the values obtained by calculation using the various models of spectroscopy are listed in Table V. As with the B(E2) value of the $3^+;0$ state in ^{6}Li, a substantial renormalization is needed in all of the models to reproduce the measure value. That is in contrast to the results of their use in an analysis of the longitudinal form factor; a contrast that is illustrated in the analysis of the transverse inelastic scattering form factor as well. The results of our calculations of the transverse form factor are compared with the data of Lichtenstadt *et al.* [37] (circles) and of van Niftrik *et al.* [38] (squares) in Fig. 9(b). All of our results reproduce the magnitude and shape of this form factor up to 3 fm^{-1}, with but a slight overestimation above 1 fm^{-1}. This suggests that no renormalization is required with any of those wave functions. The relative contributions from the $M1$ and $E2$ multipoles to this transverse form factor are shown in Fig. 9(c). Therein, and only for the $(0+2+4)\hbar\omega$ model, the total form factor is displayed by the solid line, while the $M1$ and $E2$ components are displayed by the dashed and dot-dashed lines respectively. The $M1$ component dominates the form factor below 1 fm^{-1}, above which the $E2$ component becomes much stronger. The $M1$ component dominates again above 2.5 fm^{-1}.

The results of our DWA calculations of the inelastic scattering of 200 MeV protons exciting the $\frac{1}{2}^-$ (0.478 MeV) state in ^{7}Li are compared with the data of Glover *et al.* [39] in Fig. 10. Therein, the cross sections are displayed in the top segments and the analyzing powers are shown in the bottom ones. Again the results obtained by using HO wave functions are displayed on the left while those obtained using the WS wave functions are given in the right. For this transition, the $(0+2)\hbar\omega$ and $(0+2+4)\hbar\omega$ structures give quite similar results, and are in best agreement with observation. This is due to the enhancement of the $I = 2$ multipole contributions within the larger space structures; the multipole that dominates all calculated results above 15°. The $I = 1$ amplitudes are changed little by the increase in the size of the model space but we note that they are important in the predictions of the data at small scattering angles.

The inelastic electron scattering form factors to the $\frac{7}{2}^-$ (4.63 MeV) state in ^{7}Li are displayed in Fig. 11. The longitudinal form factor data of Lichtenstadt *et al.* [41] (circles), Hutcheon and Caplan [34] (squares), and Bernheim and Bishop [42] (triangles) are compared to the results of our calculations in Fig. 11(a). As with the longitudinal form factor to the $\frac{1}{2}^-$ state [Fig. 9(a)], the $0\hbar\omega$ model fails to match the magnitude of the observations. Now, however, inclusion of $2\hbar\omega$ admixtures gives the additional transition strength necessary to reproduce the data and addition of $4\hbar\omega$ admixtures does not further enhance the form factor. This is illustrated in Fig. 11(b), wherein the data are compared to the total form factor result obtained in the $(0+2+4)\hbar\omega$ space (solid line), along with the $C2$ (dashed line) and $C4$ (dotted line) components. The form factor is entirely dominated by the $C2$ component, as is also observed in the $0\hbar\omega$ and $(0+2)\hbar\omega$ model calculations. The addition of higher $\hbar\omega$ admixtures into the model space act as the core polarization corrections normally associated with calculations in the $0\hbar\omega$ space, and serve to enhance the $C2$ component.

There is some doubt on the measured B(E2$\downarrow$) for this transition. From the quoted γ–decay rate [14] this is 3.50 e^2 fm^4 [14], however, the source of that measurement is not given in the compilation. The value obtained from an analysis of the longitudinal inelastic electron scattering form factor is 7.5 ± 0.8 e^2 fm^4 [41]. Therein, the B(E2) value for the decay of the $\frac{7}{2}^-$ state is related to that for the $\frac{1}{2}^-$ state, which is well determined. The values obtained from the various shell models are listed in Table V. Our results obtained from the $(0+2)\hbar\omega$ and $(0+2+4)\hbar\omega$ shell models lie very close to the value obtained from the γ–decay. The B(E2$\downarrow$,q) value is displayed in Fig. 12(a), as obtained from the measured and predicted longitudinal inelastic scattering form factors. The data and the results of our calculations are displayed as for Fig. 11(a). A similar discrepancy of our results with data to those observed for the $3^+;0$ state in ^{6}Li [Fig. 3(b)] and the $\frac{1}{2}^-$ state in ^{7}Li, displayed in Fig. 12(b), is now also observed, with the data suggesting a B(E2) value of around 7 or 8 e^2 fm^4. More accurate measurements of the form factor for the $\frac{7}{2}^-$ state are necessary below $q = 0.5$ fm^{-1} in order to resolve the remaining discrepancy with the quoted γ–decay

rate.

The transverse inelastic scattering form factor to the $\frac{7}{2}^-$ state is displayed in Fig. 11(c). In this case, all of our calculations reproduce the peak magnitude and position of the data of Lichtenstadt *et al.* [41]. However, all of the results underpredict the data above 2 fm^{-1}. This is due in part to the form factor being dominated by the $M3$ transition as is illustrated in Fig. 11(d), wherein the components of the Z4 calculation are displayed. The $M3$ form factor dominates, with the $E2$ contribution being a factor of 2 less. The $M5$ form factor is orders of magnitude below and, like the $E4$ contribution, may be neglected at low momentum transfer. Above 3 fm^{-1}, the $M5$ contribution becomes more important than the $E2$, and the form factor is dominated purely by the magnetic components. As such, MEC effects are expected to become significant in that regime, and their neglect is reflected by the underestimation of the form factor.

The results for the excitation of the $\frac{7}{2}^-$ in ^{7}Li by the scattering of 200 MeV protons are given in Fig. 13. Therein, the cross section and analyzing power data of Glover *et al.* [39] are compared (top and bottom sectors) to the curves identified with the same notation used in Fig. 6. As for the longitudinal inelastic electron scattering form factor, the cross section is dominated by the $I = 2$ contribution, with the contribution from the higher multipoles being negligible. Also, the $I = 2$ contribution is enhanced with the addition of higher $\hbar\omega$ admixtures to give good agreement with the data. We note that while the $I = 3$ multipole contributions are small, they are little affected with increase in the space. Higher multipoles do occur in the $(0 + 2)\hbar\omega$ and $(0 + 2 + 4)\hbar\omega$ calculations but have almost no influence in cross-section predictions.

V. CONCLUSIONS

We have obtained shell model wave functions for ^{6,7}Li in $0\hbar\omega$, $(0 + 2)\hbar\omega$, $(0 + 2 + 4)\hbar\omega$, and $(0 + 2 + 4 + 6)\hbar\omega$ spaces using existing phenomenological and G-matrix interactions. Beyond the simple $0\hbar\omega$ picture of these $0p$-shell nuclei, elements of "clustering" may be

introduced, as the larger multi-$\hbar\omega$ spaces allow for interactions (particle exchange) between the $0s$-shell α-particle and the clusters formed by the valence $0p$-shell particles. As such we have used these wave functions in calculations of ground state properties and in analyses of electron and proton scattering observables to determine to what degree this "clustering" is present in those shell model wave functions.

While the predicted r.m.s. radii for both ^{6}Li and ^{7}Li are insensitive to the size of the model space, and which adequately reproduce the measured values, it is in the magnetic dipole and quadrupole moments in which we see dramatic convergence towards the experimental values as the size of the model space is increased. However, this convergence is by no means complete. There is still some degree of renormalization necessary even in the results obtained using the $(0+2+4+6)\hbar\omega$ wave functions, while in the case of the quadrupole moments, the results obtained are still far from the experimental values. This inability to reproduce the quadrupole moment of ^{7}Li, is an indication that the shell model wave functions still do not have enough of the correlations defining the clustering.

The same is indicated especially in the analyses of the electron scattering form factors and proton scattering observables from both nuclei. In the analyses of the longitudinal inelastic electron scattering form factors and proton scattering observables for the $3^+;0$ (2.186 MeV) state in ^{6}Li and for the $\frac{1}{2}^-$ (0.478 MeV) and $\frac{7}{2}^-$ (4.63 MeV) states in ^{7}Li, none of the results of our calculations made within all the shell model spaces are able to reproduce the data at low momentum transfer. This is associated with the underestimation in the B(E2) value of each transition of about a factor of 2. Yet the high momentum transfer data for those scatterings are well reproduced when using the multi-$\hbar\omega$ wave functions. This indicates that the internal nucleon dynamics are well described, and that the asymptotics at large radius, where clustering is expected to appear, are not well reproduced. That there is remarkable agreement between experiment and theory in all of the transverse electron scattering form factors, for the calculations using the large space models, is also indicative of a reasonable description of the internal nucleon dynamics.

Our DWA analyses of the inelastic proton scattering data reveal the importance of having

large space spectroscopy. Good fits to the low excitation state data were obtained with the $(0+2)\hbar\omega$ and $(0+2+4)\hbar\omega$ OBDME in all cases, save for the $0^+;1$ excitation in ^{6}Li where the largest space OBDME lead to the best results. From our results it is clear that the prime effect of increasing the size of the model space has been to enhance the $I=2$ multipole contributions to the $3^+;0$ excitation in ^{6}Li and to the $\frac{1}{2}^-$ and $\frac{7}{2}^-$ excitation in ^{7}Li. For those transitions, other multipole contributions usually are small and little changed with structure. However, the $0^+;1$ excitation in ^{6}Li is purely $I=1$ and for this the best result is that obtained from the $(0+2+4)\hbar\omega$ model space.

ACKNOWLEDGMENTS

This research was supported by NSF Grant No. PHY94-03666 (MSU). Support was also provided by a research grant from the Australian Research Council.

REFERENCES

[1] K. Wildemuth and Y. C. Tang, *A Unified Theory of the Nucleus* (Academic Press, 1977).

[2] K. Langanke, Adv. in Nucl. Phys. **21**, 85 (1994), and references cited therein.

[3] N. W. Schellingerhout, L. P. Kok, S. A. Coon, and R. M. Adam, Phys. Rev. C **48**, 2714 (1993).

[4] D. C. Zheng, B. R. Barrett, J. P. Vary, W. C. Haxton, and C.-L. Song, Phys. Rev. C **52**, 2488 (1995).

[5] A. Arima, H. Horiuchi, K. Kubodera, and N. Takigawa, Adv. in Nucl. Phys. **5**, 345 (1972).

[6] S. Karataglidis, P. J. Dortmans, K. Amos, and R. de Swiniarski, Phys. Rev. C **52**, 861, 3224 (1995); *ibid.* **53**, 838 (1996).

[7] A. A.Korsheninnikov, *et al.*, Phys. Rev. C **53**, R537 (1996).

[8] I. Tanihata, private communication.

[9] S. Cohen and D. Kurath, Nucl. Phys. **73**, 1 (1965).

[10] E. K. Warburton and D. J. Millener, Phys. Rev C **39**, 1120 (1989).

[11] P. Navrátil and B. R. Barrett, Phys. Rev. C **54**, 2986 (1996).

[12] D. C. Zheng, private communication.

[13] OXBASH-MSU (the Oxford-Buenos-Aries-Michigan State University shell model code), A. Etchegoyen, W. D. M. Rae, and N. S. Godwin (MSU version by B. A. Brown, 1986); B. A. Brown, A. Etchegoyen, and W, D. M Rae, MUSCL Report No. 524, 1986 (unpublished).

[14] F. Ajzenberg-Selove, Nucl. Phys. **A490**, 1 (1988).

[15] T. deForest, Jr. and J. D. Walecka, Adv. Phys. **15**, 1 (1966).

[16] J. L. Friar and W. C. Haxton, Phys. Rev. C **31**, 2027 (1985).

[17] S. Karataglidis, P. Halse, and K. Amos, Phys. Rev. C **51**, 2494 (1995).

[18] J. Dubach, J. H. Koch, and T. W. Donnelly, Nucl. Phys. **A271**, 279 (1976).

[19] S. Karataglidis, MSUCL Report No. 1018, 1996 (unpublished).

[20] P. J. Dortmans and K. Amos, J. Phys. **G17**, 901 (1991); Phys. Rev. C **49**, 1309 (1994).

[21] M. Lacombe, B. Loiseau, J. M. Richard, R. Vinh Mau, J. Côté, P. Pirès, and R. de Tourreil, Phys. Rev. C **21**, 861 (1980).

[22] P. J. Dortmans and K. Amos, University of Melbourne preprint UM–P–95/41, 1995 (unpublished).

[23] J. Raynal, computer code DWBA (NEA1209/02).

[24] C. W. de Jager, H. de Vries, and C. de Vries, Atomic Data and Nuclear Data Tables **14**, 479 (1974).

[25] I. S. Towner, Phys. Rep. **155**, 263 (1987), and private communication.

[26] L. R. Suelzle, M. R. Yearian, and Hall Crannell, Phys. Rev. **162**, 992 (1967).

[27] G. C. Li, I. Sick, R. R. Whitney, and M. R. Yearian, Nucl. Phys. **A162**, 583 (1971).

[28] J. C. Bergstrom, S. B. Kowalski, and R. Neuhausen, Phys. Rev. C **25**, 1156 (1982).

[29] L. Lapikás, in *Proceedings of the Conference on Modern Trends in Elastic Electron Scattering, Amsterdam*, edited by C. de Vries (NIKHEF-K, Amsterdam, 1978), p. 49.

[30] C. W. Glover *et al*, Phys. Rev. C **41**, 2487 (1990); J. R. Comfort, private communication.

[31] J. C. Bergstrom, U. Deutschmann, and R. Neuhausen, Nucl. Phys. **A327**, 439 (1979).

[32] R. Yen, L. S. Cardman, D. Kalinsky, J. R. Legg, and C. K. Bockelman, Nucl. Phys. **A235**, 135 (1974).

[33] J. C. Bergstrom and E. L. Tomusiak, Nucl. Phys. **A262**, 196 (1976).

[34] R. M. Hutcheon and H. S. Caplan, Nucl. Phys. **A127**, 417 (1969).

[35] B. A. Brown, R. Radhi, and B. H. Wildenthal, Phys. Rep. **101**, 313 (1983).

[36] J. C. Bergstrom, I. P. Auer, and R. S. Hicks, Nucl. Phys. **A251**, 401 (1975).

[37] J. Lichtenstadt, J. Alster, M. A. Moinester, J. Dubach, R. S. Hicks, G. A. Peterson, and S. Kowalski, Phys. Lett. B **219**, 394 (1989).

[38] G. J. C. van Niftrik, L. Lapikás, H. de Vries, and G. Box, Nucl. Phys. **A174**, 173 (1971).

[39] C. W. Glover *et al.*, Phys. Rev. C **43**, 1664 (1991); J. J. Kelly, private communication.

[40] R. Schiavilla, V. R. Pandharipande, and D. O. Riska, Phys. Rev. C **41**, 309 (1990).

[41] J. Lichtenstadt, J. Alster, M. A. Moinester, J. Dubach, R. S. Hicks, G. A. Peterson, and S. Kowalski, Phys. Lett. B **244**, 173 (1990).

[42] M. Bernheim and G. R. Bishop, Phys. Lett. **5**, 294 (1963).

FIGURES

FIG. 1. The results of the calculations made for the elastic electron scattering form factors for ^{6}Li. (a) The longitudinal form factor data of Suelzle *et al.* [26] (circles) and of Li *et al.* [27] (squares) are compared to the results of the calculations made using the Z4 (solid line), MK3W (dashed line), and CK (dot-dashed line) spectroscopies. (b) $C0$ (dashed line) and $C2$ (dot-dashed line) components contributing to the longitudinal form factor (solid line). (c) The transverse $M1$ form factor data of Bergstrom *et al.* [28] (circles) and of Lapikás [29] (squares) are compared to the results of the calculations made as defined in (a).

FIG. 2. The differential cross section (top) and analyzing power (bottom) from the elastic scattering of 200 MeV protons from ^{6}Li. The data of Glover *et al.* [30] are compared to the results of calculations made using WS and HO single nucleon bound state wave functions, displayed by the solid and dashed lines respectively. The results shown in the left and right hand panels were obtained using the MK3W and Z4 structure models respectively.

FIG. 3. Longitudinal inelastic electron scattering form factor to the $3^+;0$ (2.186 MeV) state in ^{6}Li (a), and the B(E2$\downarrow$,q) value, in units of e^2 fm^4, as obtained from the form factor (b). The data of Bergstrom *et al.* [31] (circles), Yen *et al.* [32] (squares), Bergstrom and Tomusiak [33] (crosses), and Hutcheon and Caplan [34] (triangles) are compared to the results of the calculations made as defined in Fig. 1(a). The B(E2$\downarrow$) value from the associated γ–decay rate [14] is displayed by the diamond data point in (b).

FIG. 4. The differential cross section (top) and analyzing power (bottom) from the inelastic scattering of 200 MeV protons from ^{6}Li exciting the $3^+;0$ (2.186 MeV) state. The data of Glover *et al.* [30] are compared to the results of the calculations made using HO and WS single-particle wave functions as defined in the text, displayed in the left and right hand panels respectively. The results of the calculations made are as defined in Fig. 1(a).

FIG. 5. Transverse $M1$ inelastic electron scattering form factor to the $0^+;1$ (3.563 MeV) state in ^{6}Li. The data of Bergstrom *et al.* (circles [31] and squares [36]) are compared to the results of the calculations made as defined in Fig. 1(a).

FIG. 6. As for Fig. 4, but for the excitation of the $0^+;1$ (3.563 MeV) state in ^{6}Li.

FIG. 7. The results of the calculations made for the elastic electron scattering form factors for ^{7}Li. (a) The longitudinal form factor data of Suelzle *et al.* [26] (circles) and Lichtenstadt *et al.* Li89 (squares) are compared to the results of the calculations made using the Z4 (solid line), MK3W (dashed line), and CK (dot-dashed line) spectroscopies. (b) $C0$ (dashed line) and $C2$ (dot-dashed line) components contributing to the longitudinal form factor (solid line), as calculated in the $(0+2+4)\hbar\omega$ model. (c) The transverse form factor data of Lichtenstadt *et al.* [37] (circles) and van Niftrik [38] (squares) are compared to the results of the calculations made as defined in (a). (d) $M1$ (dashed line) and $E2$ (dot-dashed line) contributions to the total transverse form factor (solid line), as calculated in the $(0+2+4)\hbar\omega$ model.

FIG. 8. The differential cross section (top) and analyzing power (bottom) from the elastic scattering of 200 MeV protons from ^{7}Li. The data of Glover *et al.* [39] are compared to the results of calculations made as given in Fig. 2.

FIG. 9. The inelastic electron scattering form factors to the $\frac{1}{2}^-$ (0.478 MeV) state in ^{7}Li. The data of Lichtenstadt *et al.* [37] (circles) and of van Niftrik *et al.* [38] (squares) are compared in (a) to the results of our calculations made of the longitudinal form factor, and in (b) to the results of the calculations made of the transverse form factor, both defined as in Fig. 7(a). The $M1$ (dashed line) and $E2$ (dot-dashed line) components of the total transverse form factor (solid line) are displayed in (c) as calculated in the $(0+2+4)\hbar\omega$ model.

FIG. 10. The differential cross section (top) and analyzing power (bottom) from the inelastic scattering of 200 MeV protons exciting the $\frac{1}{2}^-$ (0.478 MeV) state in ^{7}Li. The data of Glover *et al.* [39] are compared to the results of the calculations made using the various spectroscopies. The curves displayed are as defined in Fig. 4.

FIG. 11. The inelastic electron scattering form factors to the $\frac{7}{2}^-$ (4.630 MeV) state in ^{7}Li. The longitudinal form factor data of Lichtenstadt *et al.* [41] (circles), Hutcheon and Caplan [34] (squares), and Bernheim and Bishop [42] (triangles) are compared in (a) to the results of the calculations as defined in Fig. 7(a). The $C2$ (dashed line) and $C4$ (dot-dashed line) components leading to the longitudinal form factor (solid line) are displayed in (b) as calculated in the $(0+2+4)\hbar\omega$ model. The transverse form factor data of Lichtenstadt *et al.* [41] are compared in (c) to the results of the calculations made using the various spectroscopies, while in (d) the $E2$, $M3$, $E4$, and $M5$ components, as calculated in the $(0+2+4)\hbar\omega$ model, are displayed by the long-dashed, dot-dashed, dotted, and short-dashed lines respectively. The total form factor is given by the solid line.

FIG. 12. B(E2$\downarrow$,q) for the $\frac{7}{2}^-$ (4.63 MeV) (a) and the $\frac{1}{2}^-$ (0.478 MeV) (b) states in ^{7}Li. The data, as listed in Figs. 9(a) and 11(a), are compared to our results obtained using the various shell models. The measured B(E2$\downarrow$) value for the $\frac{1}{2}^-$ state in ^{7}Li [14], as determined from the γ–decay rate, is given by the diamond data point.

FIG. 13. The differential cross section (top) and analyzing power (bottom) from the inelastic scattering of 200 MeV protons exciting the $\frac{7}{2}^-$ (4.630 MeV) state in ^{7}Li. The data of Glover *et al.* [39] are compared to the results of the calculations made using the various spectroscopies as defined in Fig. 4.

TABLES

TABLE I. The low-energy spectra of ^{6}Li and ^{7}Li as calculated in the complete $0\hbar\omega$ (CK and Zheng interactions), $(0+2)\hbar\omega$ (MK3W and Zheng interactions), and $(0+2+4)\hbar\omega$ (Zheng interaction) shell models. The measured energies were obtained from Ref. [14]. All energies are in MeV.

	$J^\pi;T$	Expt.	$0\hbar\omega$		$(0+2)\hbar\omega$		$(0+2+4)\hbar\omega$
			(CK)	(Zheng)	(MK3W)	(Zheng)	(Zheng)
^{6}Li	$1^+;0$	0.000					
	$3^+;0$	2.186	2.144	2.991	2.645	2.876	2.521
	$0^+;1$	3.563	2.508	3.718	1.856	3.578	3.380
^{7}Li	$\frac{3}{2}^-;\frac{1}{2}$	0.000					
	$\frac{1}{2}^-$	0.478	1.068	0.115	0.525	0.472	0.478
	$\frac{7}{2}^-$	4.630	4.794	5.103	5.713	5.871	5.391

TABLE II. The r.m.s. radii, magnetic moments, and quadrupole moments of ^{6}Li and ^{7}Li as calculated in the complete $0\hbar\omega$, $(0+2)\hbar\omega$, $(0+2+4)\hbar\omega$, and $(0+2+4+6)\hbar\omega$ model spaces. The Zheng interaction [4,12] was used in each space. HO single particle wave functions were used with $\hbar\omega = 14$ MeV. The data are from Refs. [14] and [24].

Nucleus	Model space	r_r (fm)	μ (n.m.)	Q (e fm^2)
^{6}Li	$0\hbar\omega$	2.32	0.869	−0.264
	$(0+2)\hbar\omega$	2.27	0.848	−0.208
	$(0+2+4)\hbar\omega$	2.33	0.845	−0.012
	$(0+2+4+6)\hbar\omega$	2.36	0.840	0.017
	Expt.	2.57	0.822	−0.083
^{7}Li	$0\hbar\omega$	2.33	3.024	−1.68
	$(0+2)\hbar\omega$	2.26	3.057	−2.43
	$(0+2+4)\hbar\omega$	2.30	3.039	−2.63
	$(0+2+4+6)\hbar\omega$	2.32	3.006	−2.85
	Expt.	2.41	3.256	−4.06

TABLE III. As for Table II, but using the CK, MK3W, and Zheng interactions in the complete $0\hbar\omega$, $(0+2)\hbar\omega$, and $(0+2+4)\hbar\omega$ model spaces respectively.

Nucleus		Interaction			
		CK	MK3W	Zheng	Expt.
^{6}Li	$r_{r.m.s.}$ (fm)	2.33	2.51	2.33	2.57
	μ (n.m.)	0.834	0.770	0.845	0.822
	Q (e fm^2)	−0.78	−1.98	−0.012	−0.083
^{7}Li	$r_{r.m.s.}$ (fm)	2.33	2.46	2.30	2.41
	μ (n.m.)	3.171	3.192	3.039	3.256
	Q (e fm^2)	−1.84	−3.21	−2.63	−4.06

TABLE IV. Harmonic oscillator energies and parameters for the Woods-Saxon potential for the single particle wave functions in ^{6,7}Li.

Nucleus	Model	$\hbar\omega$ (MeV)	V_0 (MeV)	r_0 (fm)	a (fm)	λ
^{6}Li	CK	14.53	-54.5	1.35	0.65	7.0
	MK3W	15.06	-54.5	1.35	0.65	7.0
	Z4	12.65	-43.0	1.70	0.65	7.0
^{7}Li	CK	15.06	-54.5	1.35	0.65	7.0
	MK3W	16.02	-54.5	1.35	0.65	7.0
	Z4	13.39	-49.5	1.55	0.65	7.0

TABLE V. B(E2↓) values (in units of e^2 fm^4) for the transitions in ^{6,7}Li as listed. The HO single particle wave functions used were those given in Table IV.

Nucleus	Transition	$0\hbar\omega$		$(0+2)\hbar\omega$		$(0+2+4)\hbar\omega$	Expt. [14]
		CK	Zheng	MK3W	Zheng		
^{6}Li	$3^+;0 \rightarrow$ g.s.	2.65		4.31		4.07	9.3 ± 2.1
^{7}Li	$\frac{1}{2}^- \rightarrow$ g.s.	3.04	2.51	8.00	6.21	7.23	16.4 ± 1.0
	$\frac{7}{2}^- \rightarrow$ g.s.	1.04	1.30	3.30	2.88	3.32	$3.50, 7.5 \pm 0.8$[a]

a) Ref. [41].

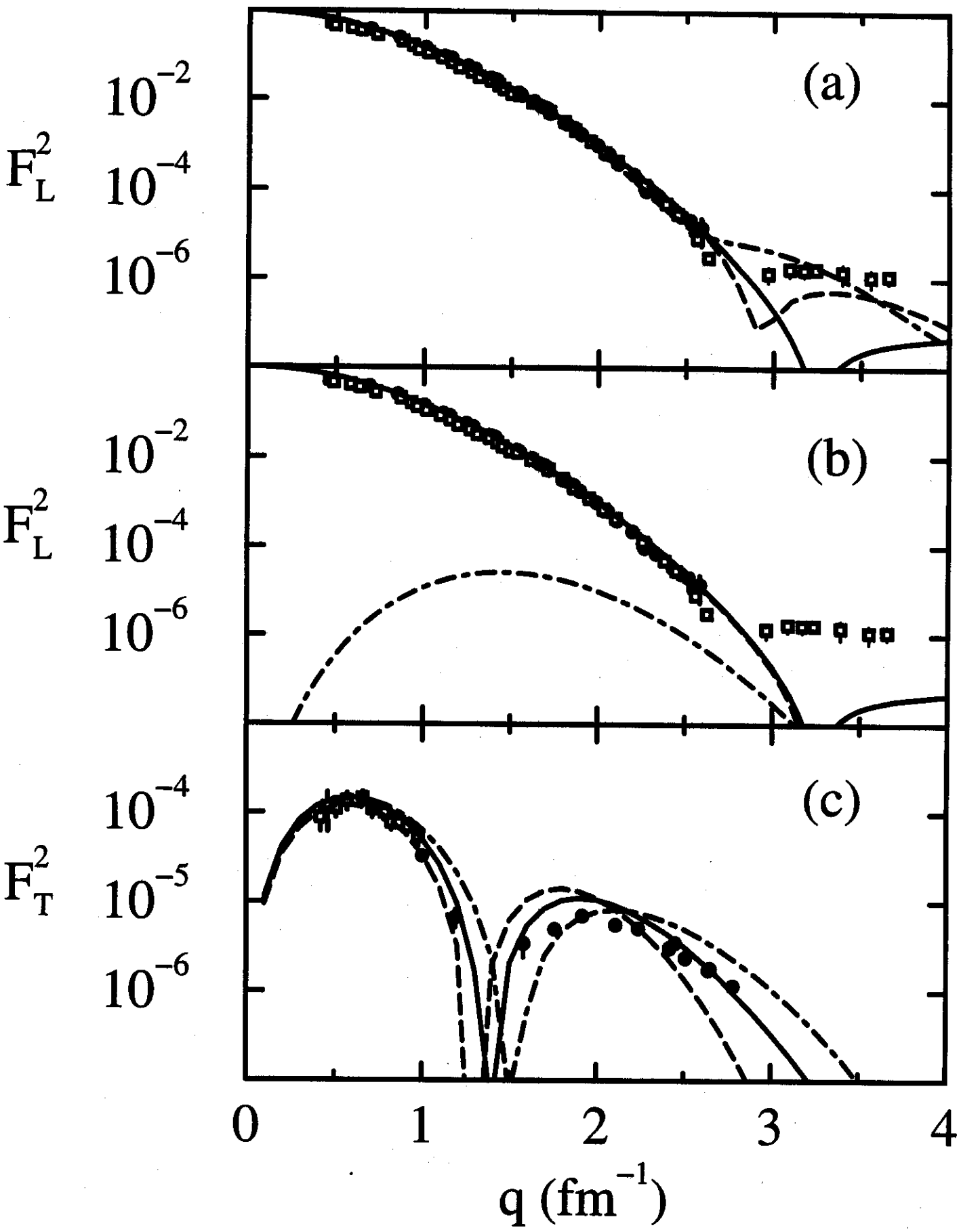

FIG. 1

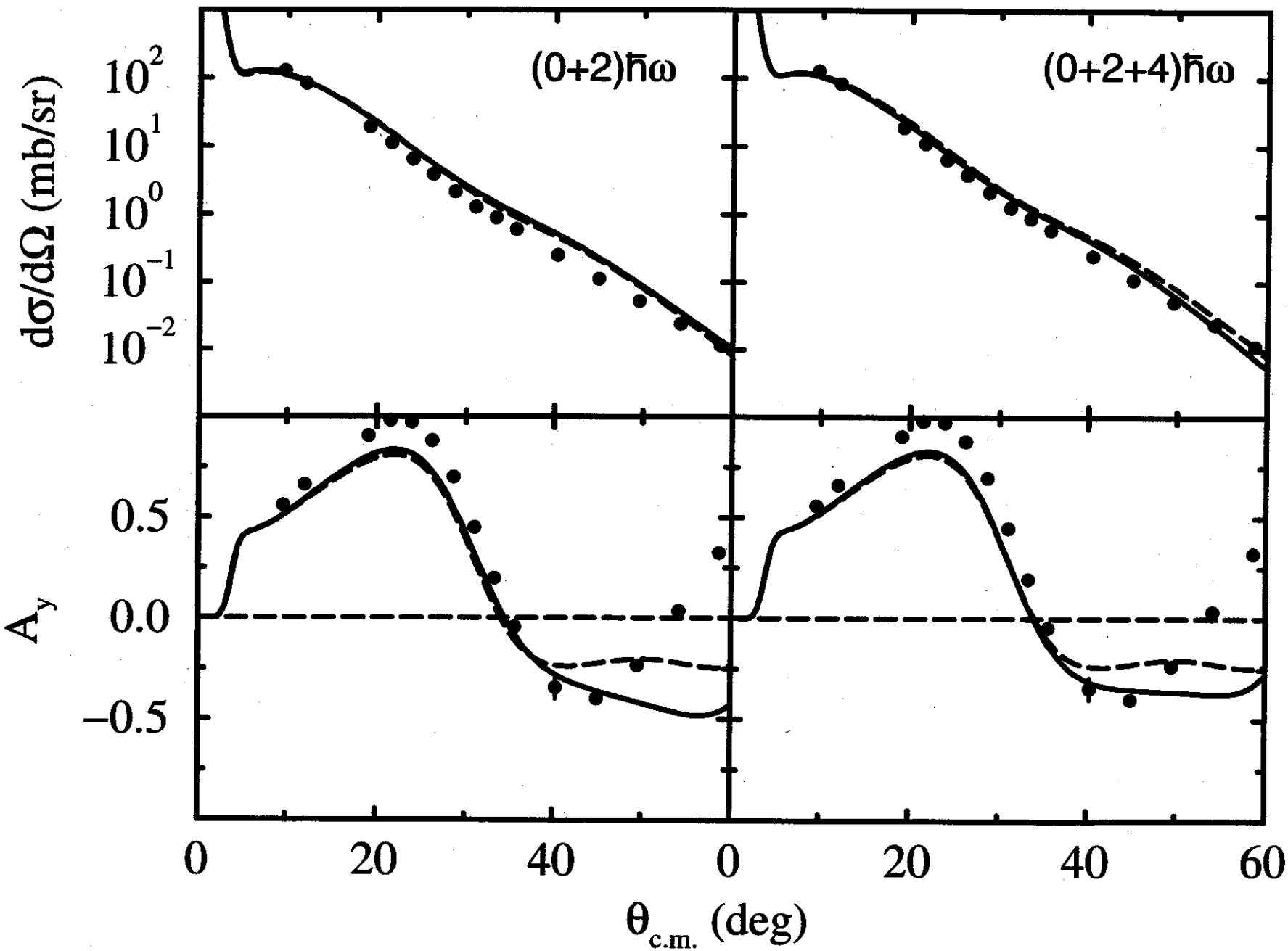
(0+2)ħω
(0+2+4)ħω
dσ/dΩ (mb/sr)
10^2
10^1
10^0
10^{-1}
10^{-2}
A_y
0.5
0.0
−0.5
0
20
40
0
20
40
60
$\theta_{c.m.}$ (deg)

Fig. 2

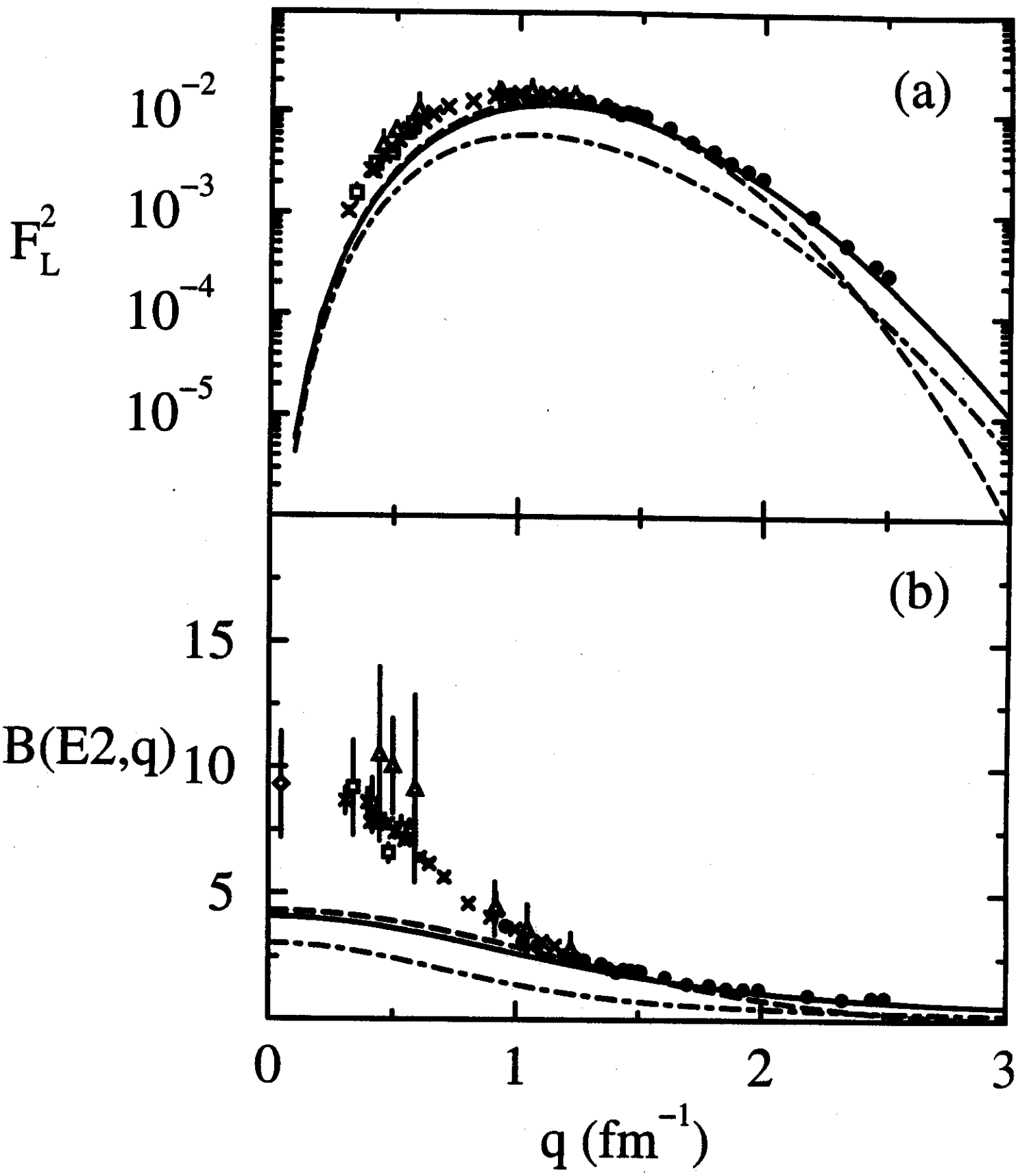

FIG. 3

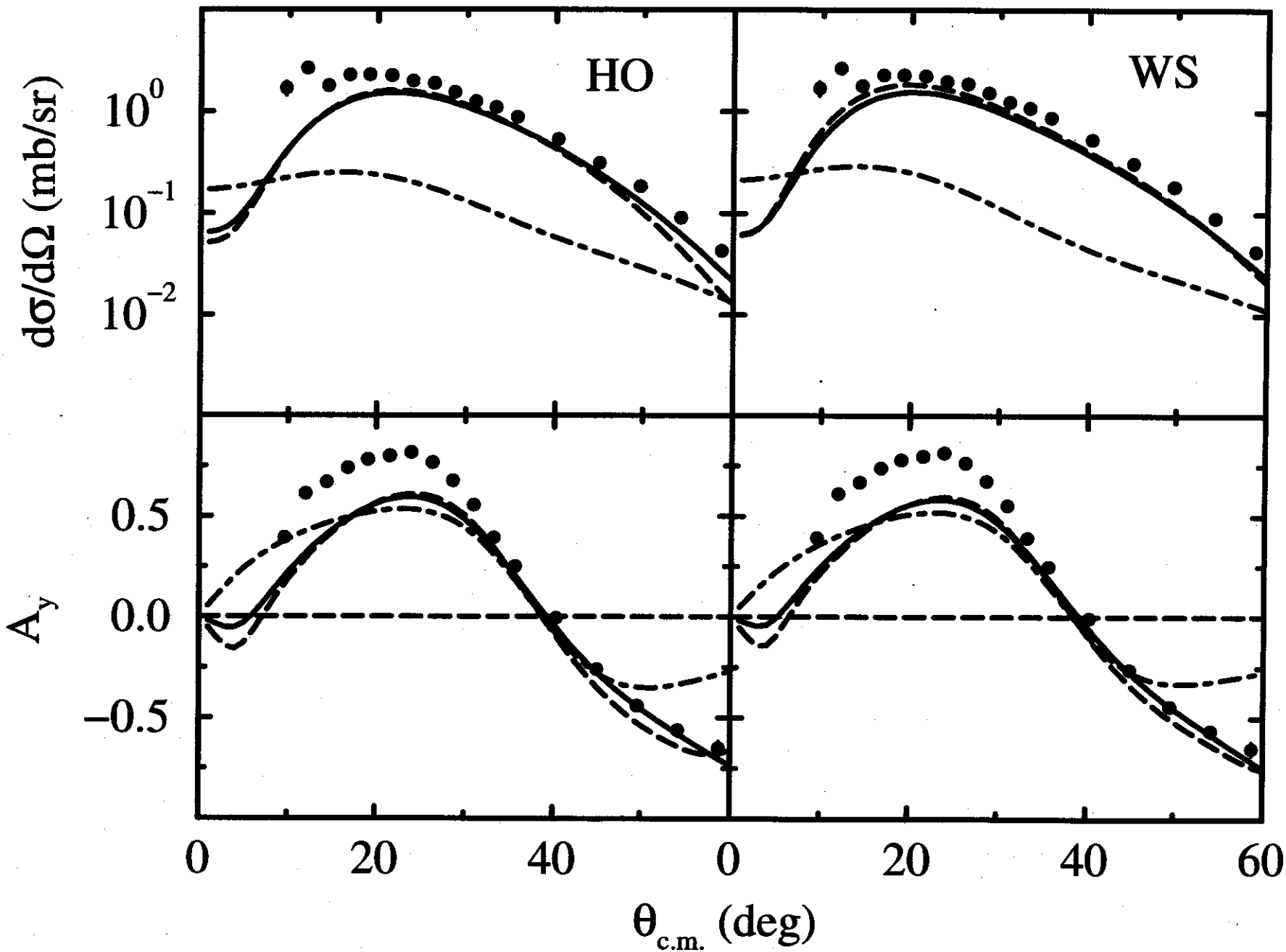

Fig. 4

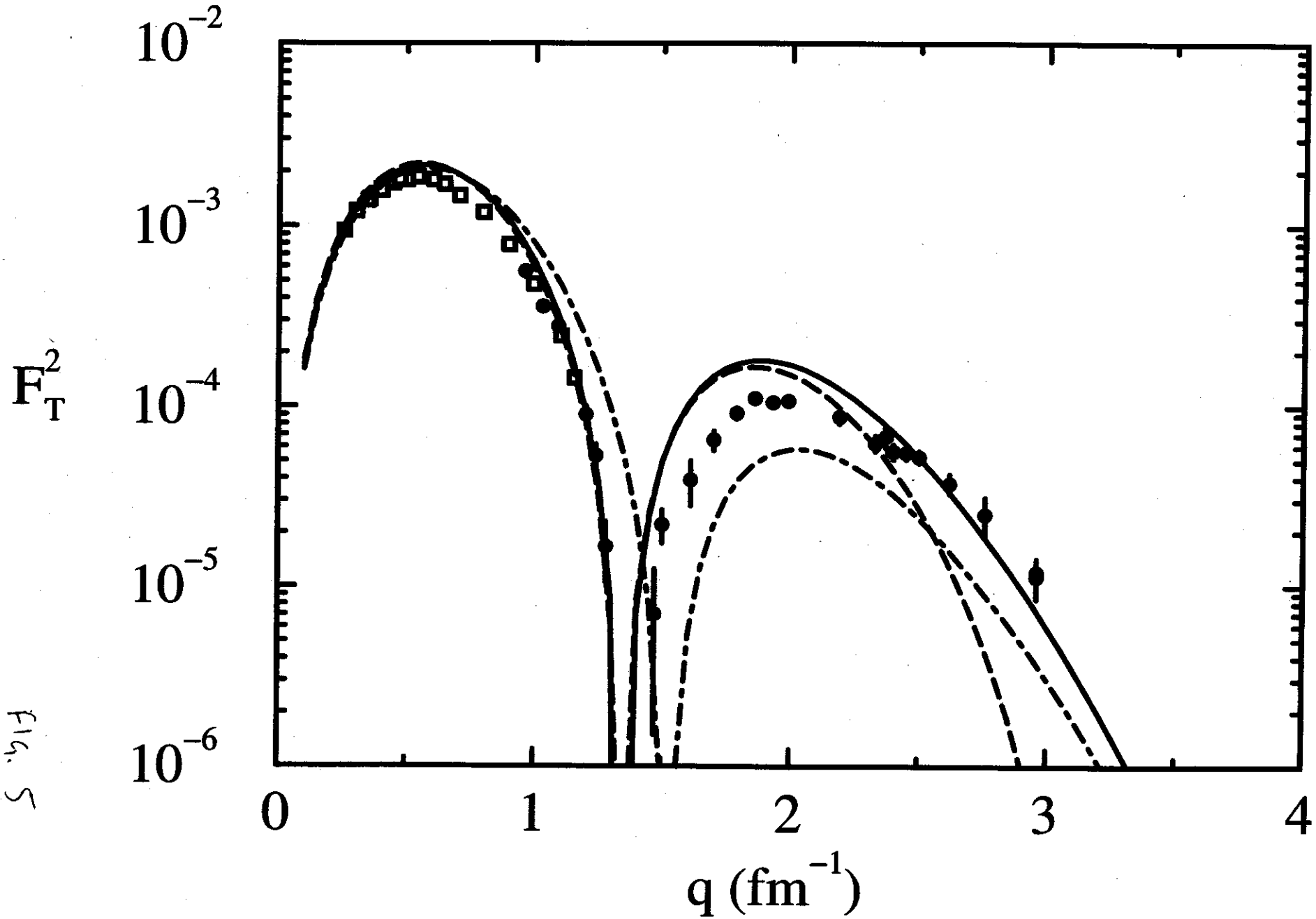

Fig. 5

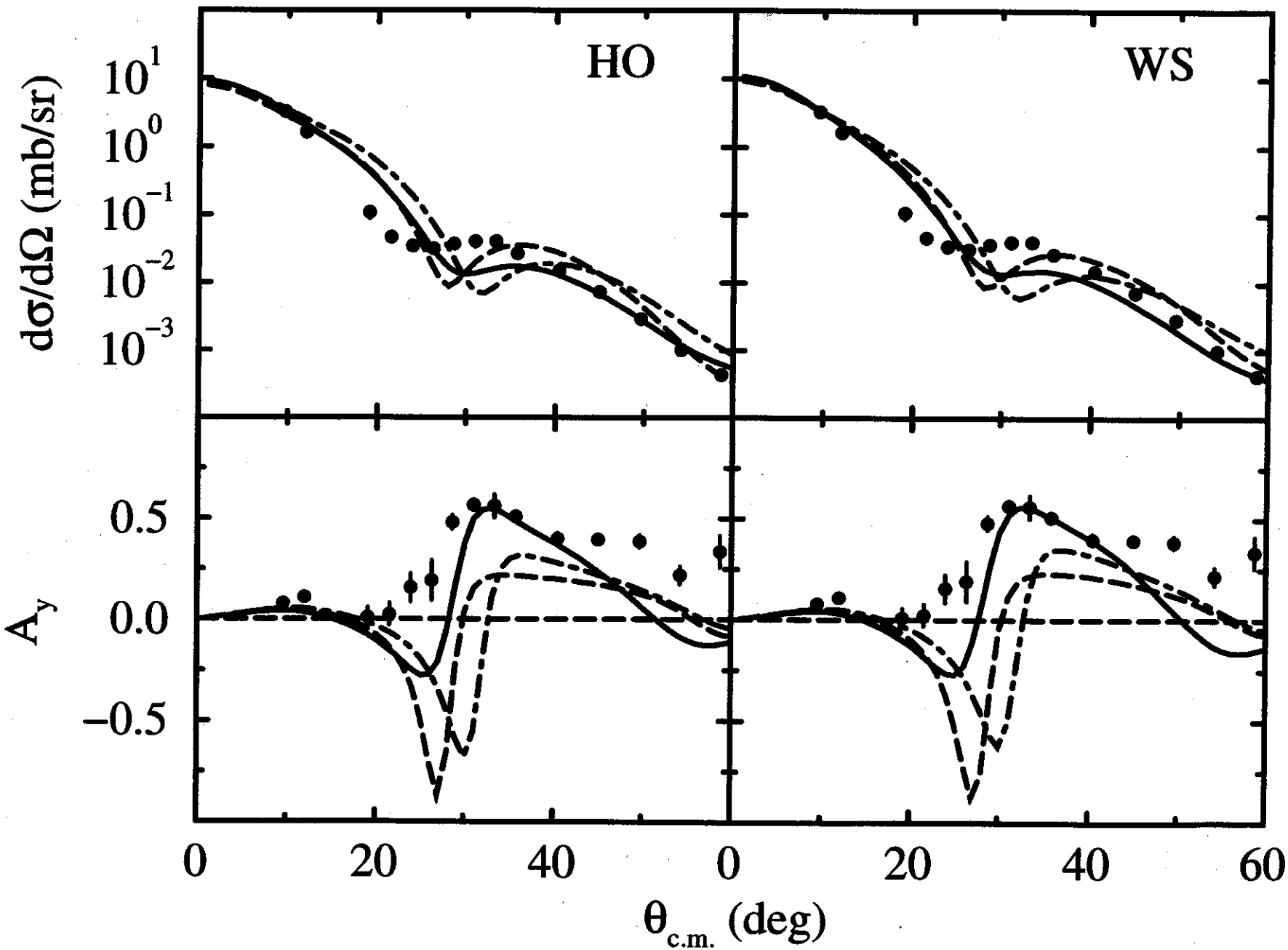
HO
WS
dσ/dΩ (mb/sr)
10^{1}
10^{0}
10^{-1}
10^{-2}
10^{-3}
A_y
0.5
0.0
−0.5
0
20
40
0
20
40
60
$\theta_{c.m.}$ (deg)

Fig. 6

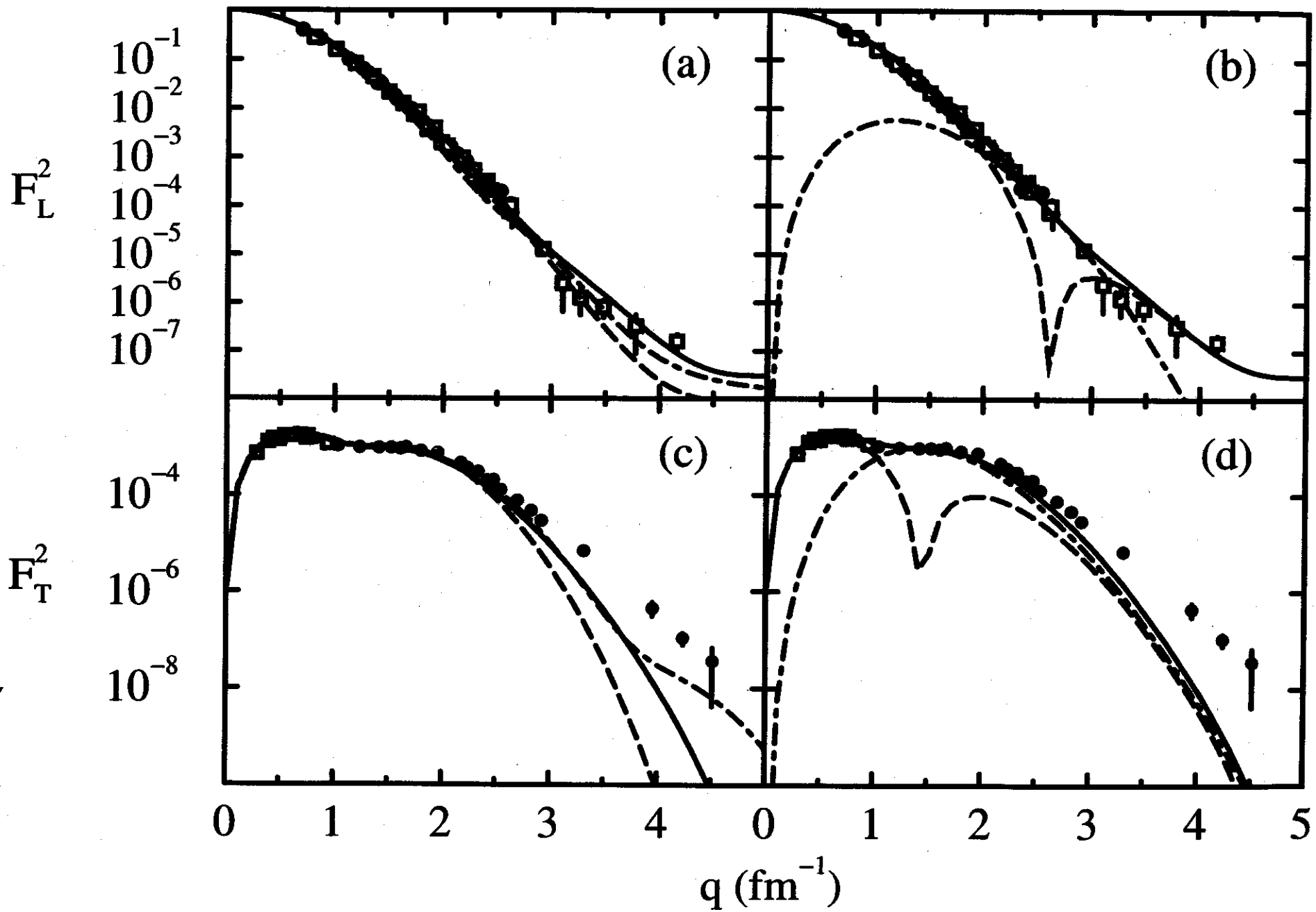
(a)
(b)
(c)
(d)
F_L^2
F_T^2
10^{-1}
10^{-2}
10^{-3}
10^{-4}
10^{-5}
10^{-6}
10^{-7}
10^{-4}
10^{-6}
10^{-8}
0 1 2 3 4 0 1 2 3 4 5
q (fm^{-1})

FIG. 7

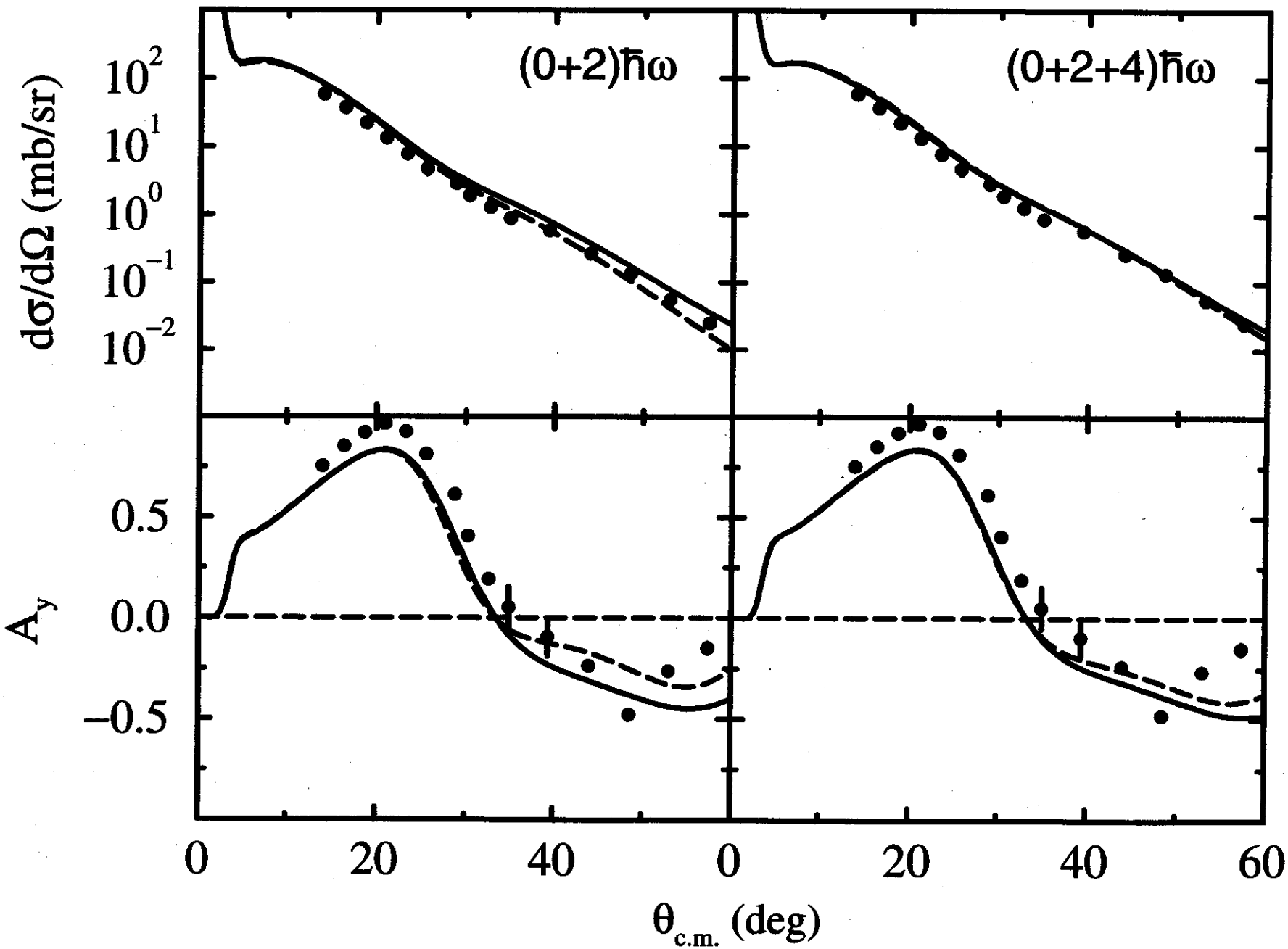
(0+2)ħω
(0+2+4)ħω
dσ/dΩ (mb/sr)
10^2
10^1
10^0
10^{-1}
10^{-2}
A_y
0.5
0.0
−0.5
0
20
40
0
20
40
60
$\theta_{c.m.}$ (deg)

Fig. 8

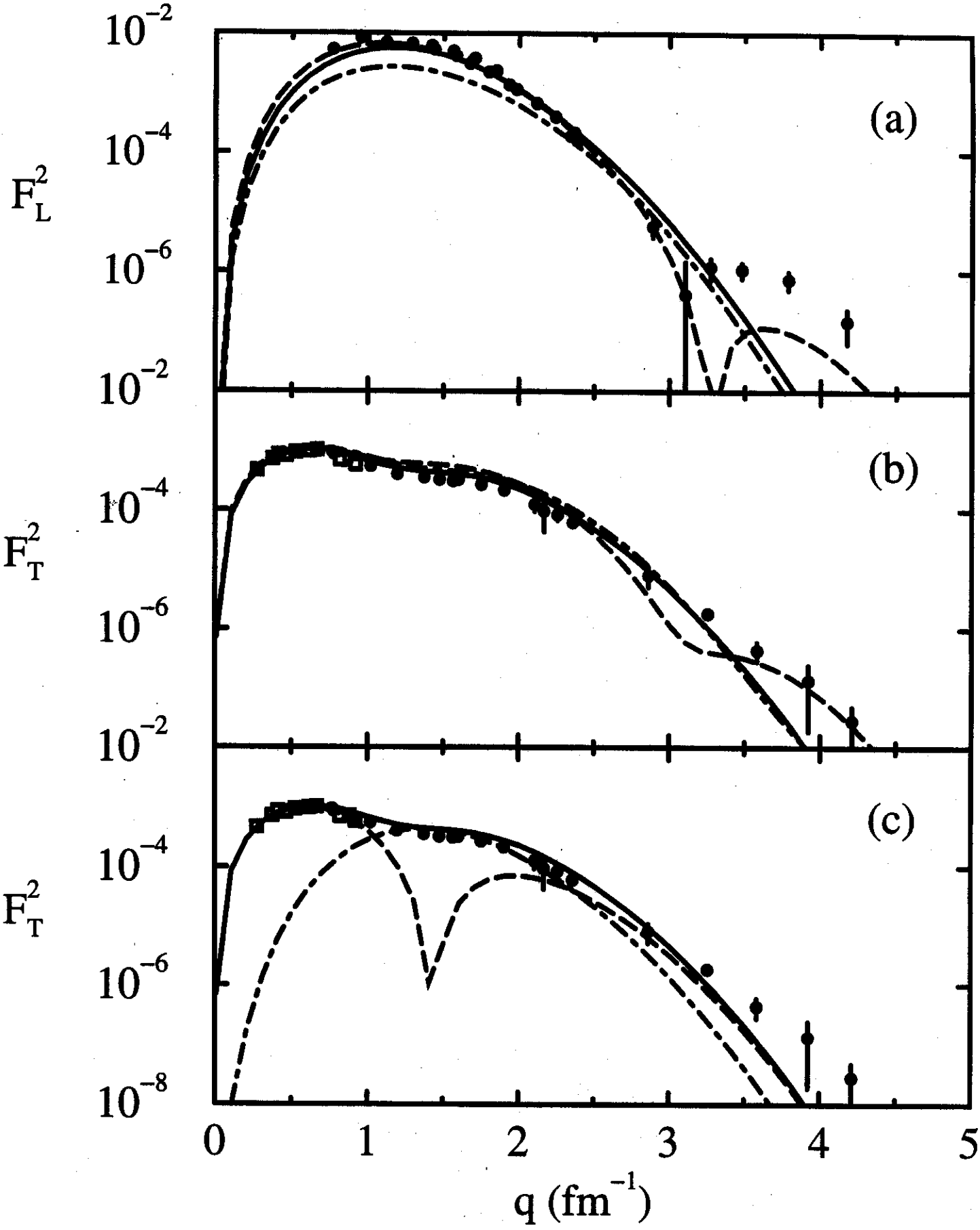
10^{-2}
10^{-4}
10^{-6}
10^{-2}
F_L^2
(a)
10^{-4}
10^{-6}
10^{-2}
F_T^2
(b)
10^{-4}
10^{-6}
10^{-8}
F_T^2
(c)
0
1
2
3
4
5
q (fm^{-1})

FIG. 9

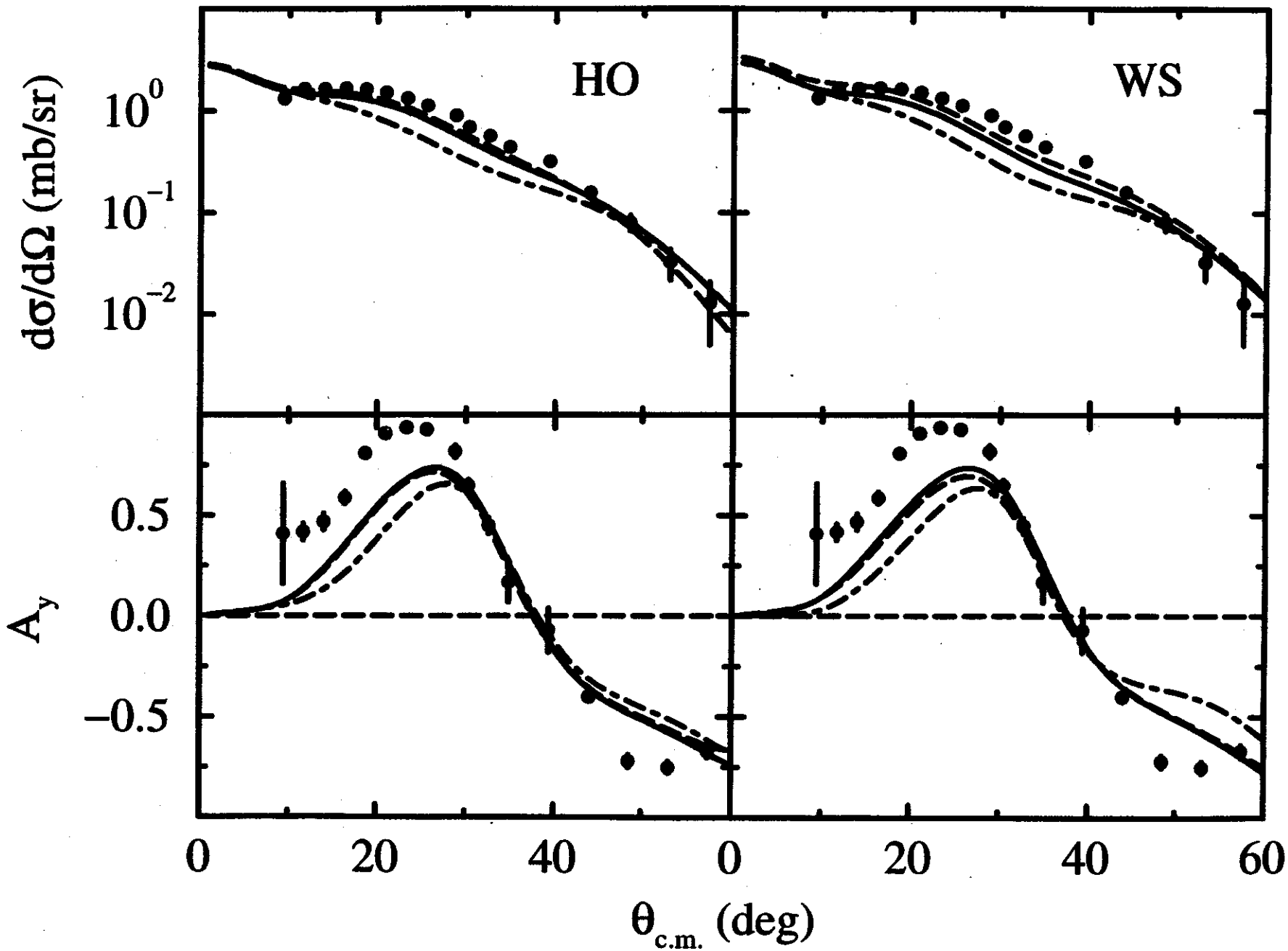

Fig. 10

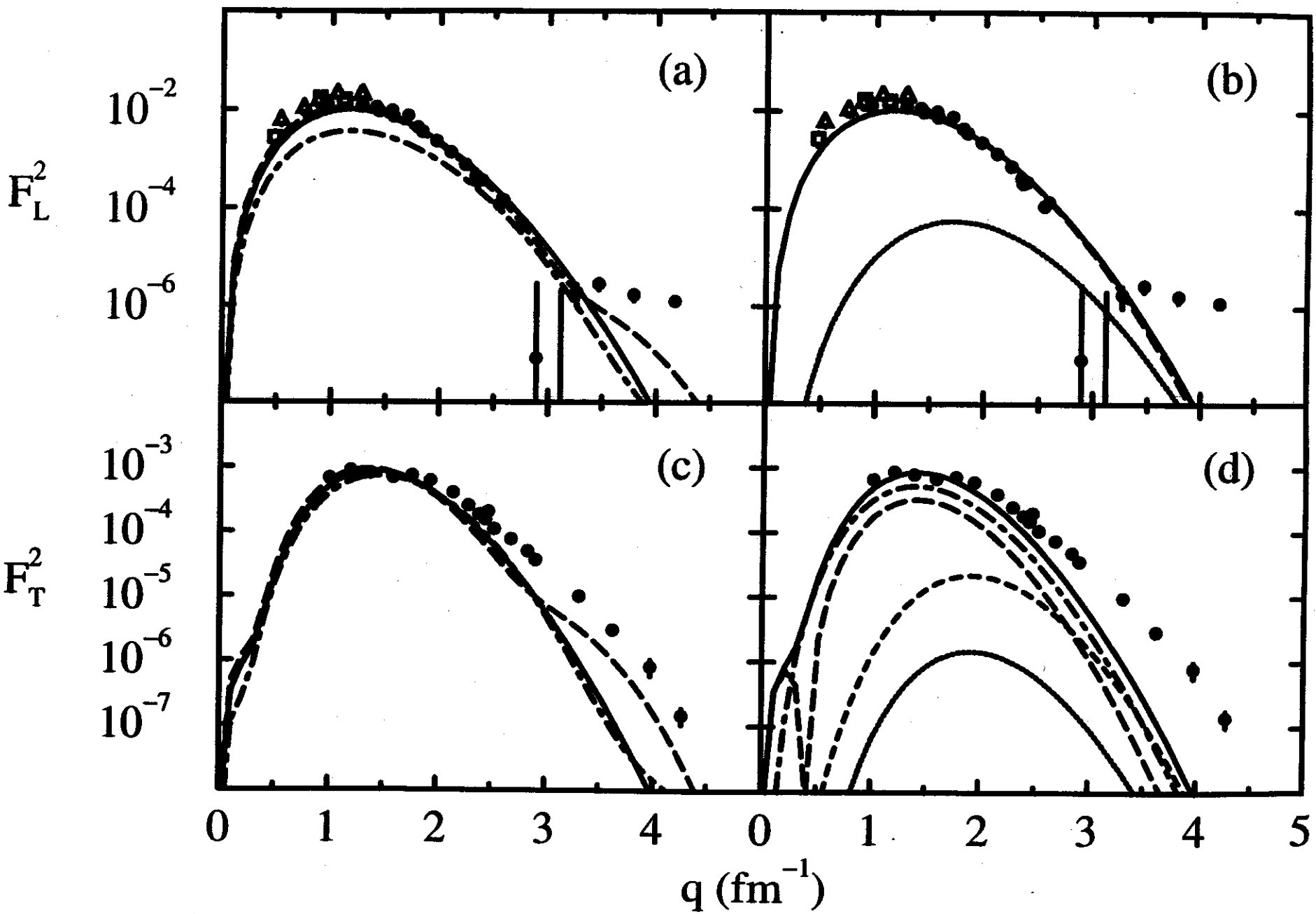

FIG. 11

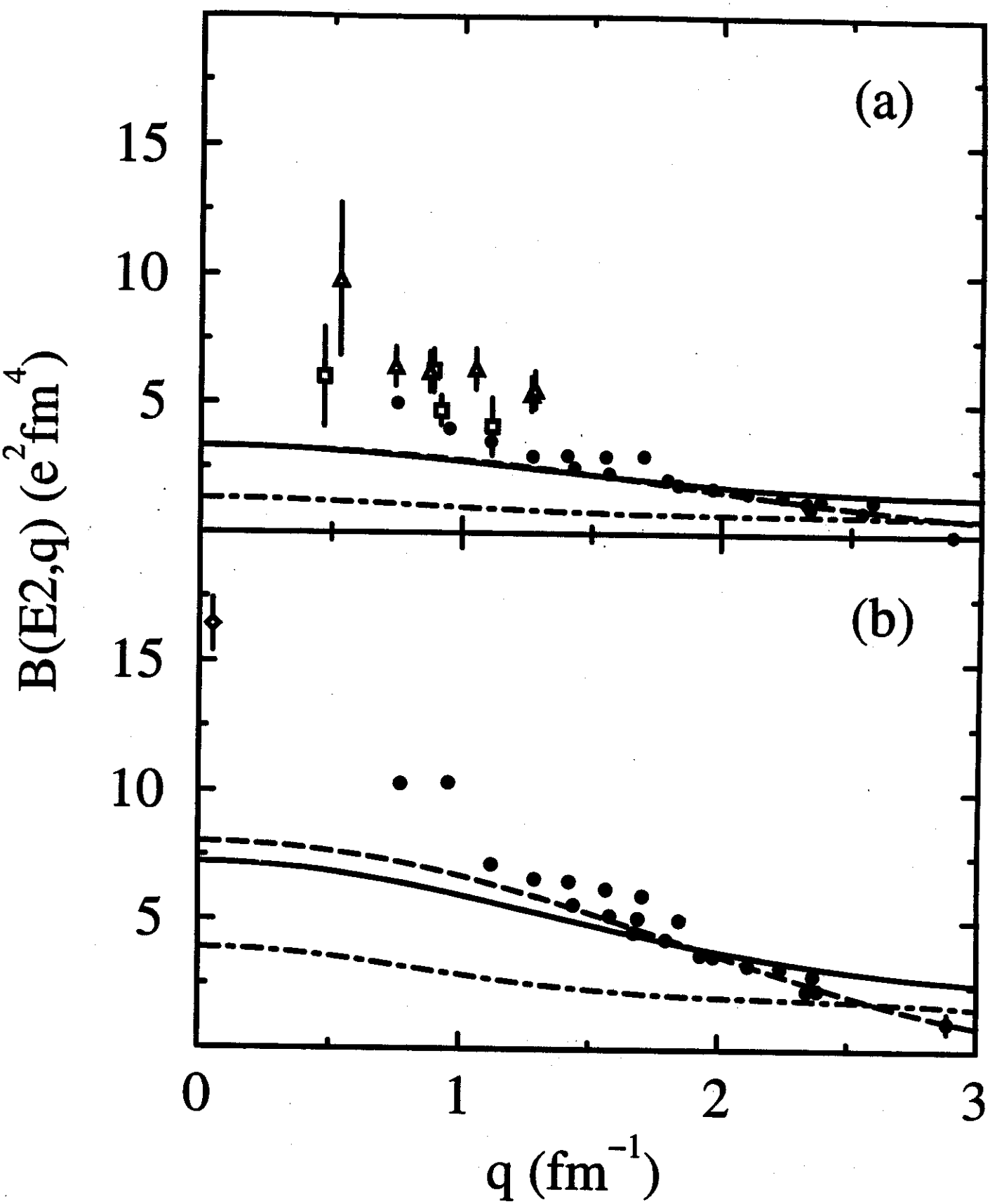

FIG. 12

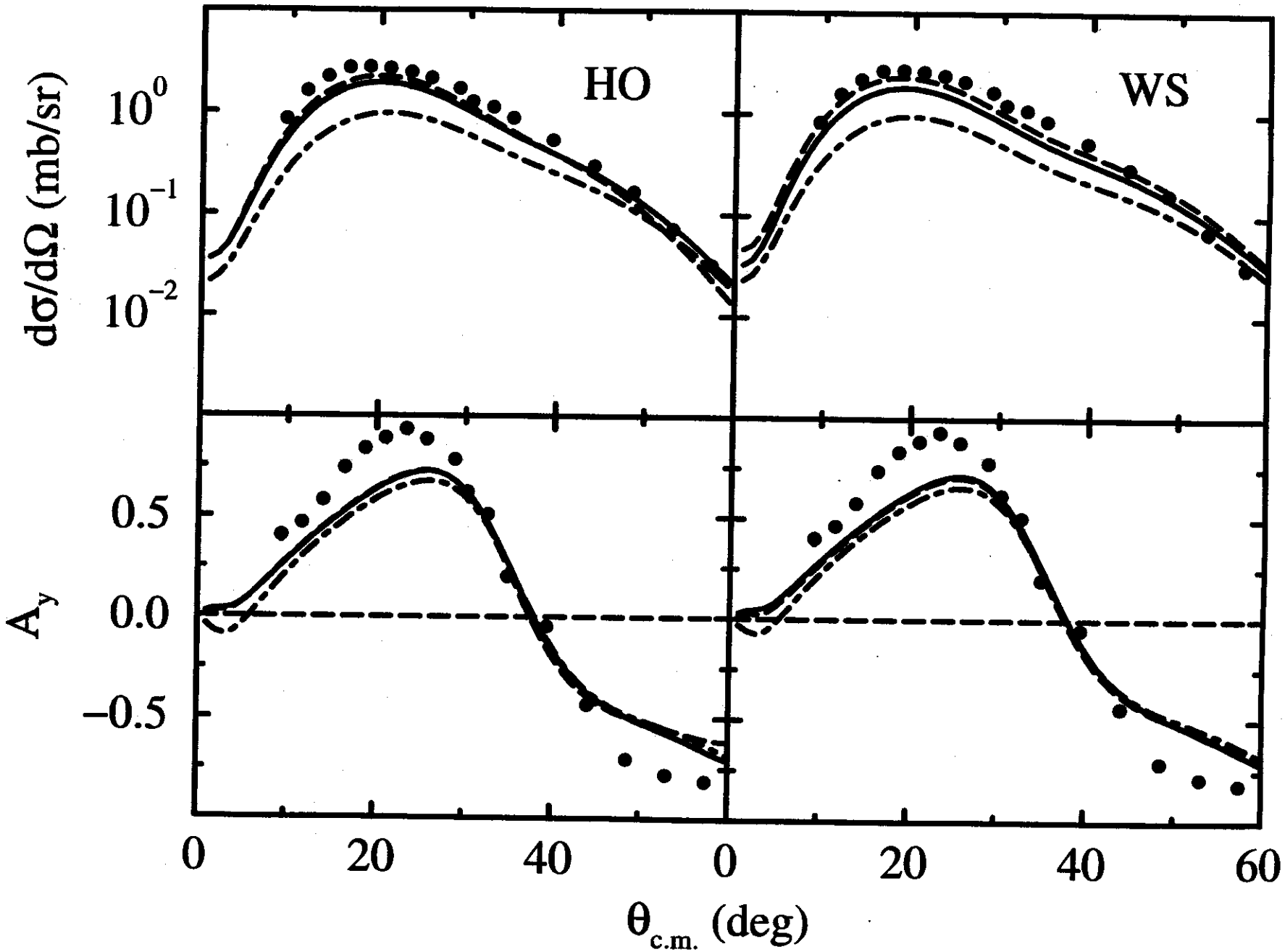

Fig. 13